INVITED PAPER

Silicon Nitride in Silicon Photonics

By Daniel J. Blumenthal, *Fellow IEEE*, René Heideman, Douwe Geuzebroek, Arne Leinse, and Chris Roeloffzen

ABSTRACT | The silicon nitride (Si_3N_4) planar waveguide platform has enabled a broad class of low-loss planar-integrated devices and chip-scale solutions that benefit from transparency over a wide wavelength range (400–2350 nm) and fabrication using wafer-scale processes. As a complimentary platform to silicon-on-insulator (SOI) and III–V photonics, Si_3N_4 waveguide technology opens up a new generation of system-on-chip applications not achievable with the other platforms alone. The availability of low-loss waveguides (<1 dB/m) that can handle high optical power can be engineered for linear and nonlinear optical functions, and that support a variety of passive and active building blocks opens new avenues for system-on-chip implementations. As signal bandwidth and data rates continue to increase, the optical circuit functions and complexity made possible with Si_3N_4 has expanded the practical application of optical signal processing functions that can reduce energy consumption, size and cost over today's digital electronic solutions. Researchers have been able to push the performance photonic-integrated components beyond other integrated platforms, including ultrahigh Q resonators, optical filters, highly coherent lasers, optical signal processing circuits, nonlinear optical devices, frequency comb generators, and biophotonic system-on-chip. This review paper covers the history of low-loss Si_3N_4 waveguide technology and a survey of worldwide research in a variety of device and applications as well as the status of Si_3N_4 foundries.

KEYWORDS | Biophotonics; lasers; microwave photonics; optical device fabrication; optical fiber devices; optical filters; optical resonators; optical sensors; optical waveguides; photonic-integrated circuits; quantum entanglement; silicon nitride; silicon photonics; spectroscopy

I. INTRODUCTION

Photonic-integrated circuits (PICs) are poised to enable an increasing number of applications including data communications and telecommunications [1], [2], biosensing [3], positioning and navigation [4], low noise microwave synthesizers [5], spectroscopy [6], radio-frequency (RF) signal processing [7], quantum communication [8], and atomic clocks [9]. Emerging system-on-chip applications are driving the demand for PICs that operate over an unprecedented optical bandwidth range, from the visible wavelength (~400 nm) out to beyond the infrared (>2.3 μm), and deliver performance previously only achievable with bulk optic technologies.

In this paper, we review the history and state of the art in silicon nitride (Si_3N_4) photonics, a third integration platform that is complimentary in characteristics and performance to the silicon-on-insulator (SOI) photonics and group III–V photonics platforms and is compatible with foundry-scale processes. Si_3N_4 PIC technology offers low optical attenuation, from the visible to beyond the infrared, a range not accessible with the other platforms. Today, SOI offers large volume photonic integration through traditional complementary metal–oxide–semiconductor (CMOS) infrastructure. Traditional SOI photonics employs high-contrast waveguides formed from a silicon core surrounded by oxide cladding, keeping the light tightly confined to the core [1]. These strongly confining waveguides lead to very compact photonic circuits

Manuscript received February 19, 2018; revised July 10, 2018; accepted July 11, 2018. This work was supported in part by Defense Advanced Research Project Agency (DARPA) Microsystems Technology Office (MTO) Space and Naval Warfare Systems Center Pacific (SSC Pacific) (DoD-N W911NF-04-9-0001 iPhoD HR0011-09-C-01233, EPHI HR0011-12-C-0006, iWOG HR0011-14-C-0111, PRIGM:AIMS N66001- 16-C-4017) and Keysight Technologies. The views and conclusions contained in this document are those of the authors and should not be interpreted as representing official policies of the Defense Advanced Research Projects Agency or the U.S. Government or KeySight Technologies. *(Corresponding author: Daniel J. Blumenthal.)*

D. J. Blumenthal is with the Department of Electrical and Computer Engineering, University of California–Santa Barbara, Santa Barbara, CA 93106 USA (e-mail: danb@ucsb.edu).

R. Heideman, **D. Geuzebroek**, **A. Leinse**, and **C. Roeloffzen** are with LioniX International BV, 7521 AN Enschede, The Netherlands (e-mail: r.g.heideman@lionix-int.com; d.h.geuzebroek@lionix-int.com; a.leinse@lionix-int.com; c.g.h.roeloffzen@lionix-int.com).

Digital Object Identifier 10.1109/JPROC.2018.2861576

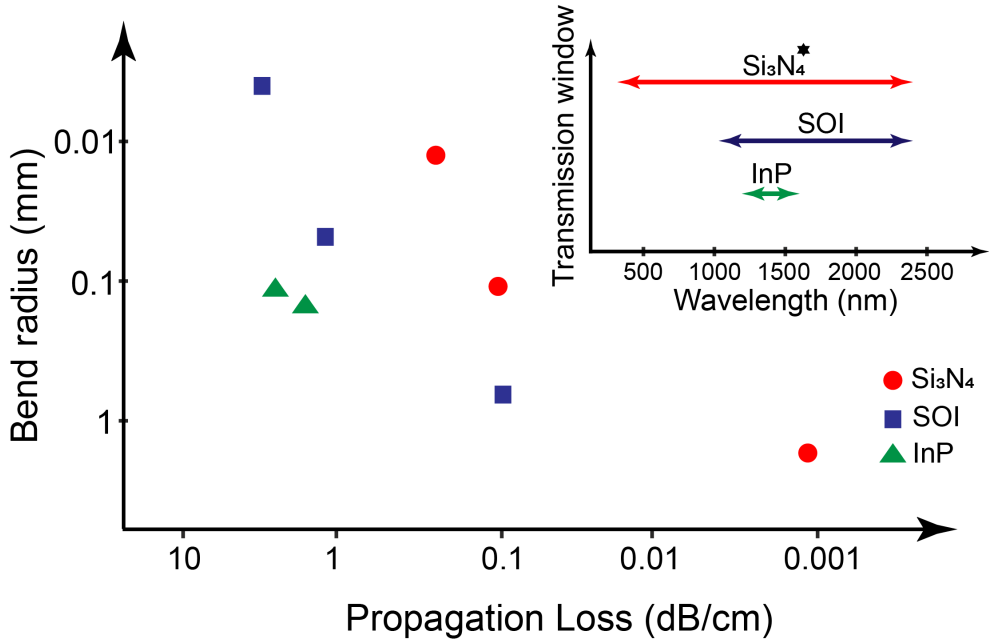

Fig. 1. ***Bend radii, propagation loss, and window of transparency for published Si_3N_4, SOI, and InP waveguides.***

with small bend radii and moderate waveguide losses on the order of 0.1 dB/cm. The widely used group III–V photonics material indium phosphide (InP) is a foundry scale process that provides waveguides with optical gain and efficient signal modulation in the telecommunications wavebands [10]. InP is used in many standalone PIC applications and as a gain block for SOI PICs with a tradeoff in higher waveguide losses (2 to 0.4 dB/cm [11]) and larger bend radii, as compared to SOI.

Si_3N_4 PIC technology provides lower loss waveguides and building blocks complimentary to SOI and III–V PICs. Si_3N_4 is traditionally used in standard CMOS processes to insulate individual transistors, known as local oxidation of silicon (LOCOS), and is also used as gate material in ion-sensitive field-effect transistors (ISFETs) purposes [12]. Optical waveguides employ a core layer of Si_3N_4 embedded in a surrounding silicon dioxide (SiO_2) cladding material. The refractive index of the cladding at 1.55-μm wavelength (1.98 for SiO_2) and core (1.45 for Si_3N_4) allows for designs that range from low- to high-contrast waveguides with low propagation losses in the range of 0.3 dB/m to 1.0 dB/cm over the range from ~400 to – 2350 nm. In general, the waveguide loss and minimum bend radius are design tradeoffs based on desired performance, footprint and optical power density, and vary for each integration platform. Fig. 1 summarizes published data on waveguide propagation loss, minimum bend radius, and wavelength operating range for Si_3N_4, SOI, and InP waveguides [13]– [15].

II. HISTORY OF Si_3N_4 INTEGRATED PHOTONICS

Si_3N_4 waveguides have been of interest since the late 1970s with several historical summaries written, including an invited article by Munoz *et al.* [16] and several articles in the recent IEEE JOURNAL ON SELECTED AREAS IN QUANTUM ELECTRONICS (IEEE JSTQE) Special Issue on Ultralow Loss Planar Waveguides and Their Applications [17]. Early motivation to investigate Si_3N_4 photonic circuits was a platform that resided on a silicon substrate, utilized compatible silicon processing technologies, and addressed applications at wavelengths where silicon is absorbing [toward the short end of infrared (IR) into the visible]. Today, a wealth of applications have emerged that leverage this third wafer-scale platform to complement the capabilities of SOI and III–V waveguide technologies.

A. The Early Days

Early work focused on fabrication of thin film slab waveguides that guided 632-nm light [18], [19] and employed Si_3N_4 cores with a silicon dioxide lower cladding layer formed on a silicon substrate. These structures were formed by thermally oxidizing silicon to form a lower waveguide cladding layer on top of the silicon substrate, followed by subsequent deposition of Si_3N_4 as the waveguide core layer. As is the case today, the thermally grown lower cladding layer thickness must be sufficient (in the several micrometers to 15-μm range) to minimize absorption in the silicon substrate, and is dependent on the optical waveguide confinement. Thermally oxidized silica remains one of the lowest loss oxide-based cladding materials due to a low surface roughness from the original high-quality silicon substrate and the absence hydrogen in the material and growth process. The higher index waveguide core is formed using deposition techniques like chemical vapor deposition (CVD) followed by patterning and etch steps to form channel waveguides.

Early devices employed an air upper cladding design, with later advancements in upper cladding oxide deposition used to reduce losses dominated by surface roughness and lithography induced waveguide scattering and material optical absorption.

One of the first reported silicon nitride/silicon dioxide (Si_3N_4/SiO_2) waveguides was a single-mode channel waveguide [20] with 1–2-dB/cm propagation loss. These early stage losses compared favorably to today's state-of-the-art SOI waveguide losses ~0.3 dB/cm [21] and optical fiber 0.4160-dB/km record loss [22]. Efforts focused on loss reduction by minimizing variations in core and upper cladding material density and lithography and etching induced waveguide roughness. Thermal annealing techniques were employed after deposition to drive out absorption impurities. Combined with improved CVD processes, record low losses (0.1 dB/cm) at the time were achieved. Annealing at elevated temperatures led to densification of the deposited films and reduced optical scattering by unwanted material clusters formed during CVD. In 1987, lower than 0.3-dB/cm loss in the communications wavebands (1.3–1.6 μm) was reported by Henry *et al.* [23]. These waveguides were designed with tightly confined optical modes for low-loss coupling to buried heterostructure semiconductor lasers. Losses in the telecommunications waveband due to hydrogen (H)-based absorption peaks at 1.52 μm (in the Si_3N_4 core) and 1.40 μm (in the SiO_2 cladding) were identified with contributions of 1.2 and 2.2 dB/cm, respectively.

In 1993, fabrication of the first Si_3N_4 PIC, designed for highly sensitive immuno-sensing [24], was reported. Detection of the presence of proteins occurred in an etched portion of the waveguide cladding, where the mode in the exposed optical core was influenced by the test material. A low-loss visible wavelength sensing interferometer on-chip demonstrated the capabilities of the emerging Si_3N_4 PIC process. By the late 1990s, process and device development in a related nitride-based material, silicon oxynitride (SiO_xN_y) [25], [26], further advanced device design and process capabilities of the nitrides as a whole. A wide range of SiO_xN_y 1550-nm telecommunications devices including filters, polarization splitters, fiber to waveguide mode transformers, tunable optical add/drop multiplexers, thermally controlled optical switches, and bus-coupled ring resonators were demonstrated.

B. The Push for Ultralow-Loss Waveguides

In 2003, the U.S. Defense Advanced Research Project Agency (DARPA) established the data in the optical domain networking (DOD-N) research program to advance integrated optical packet routing PIC technologies. The LASOR project at UCSB was funded under this program to demonstrate a photonic chip-based all-optical packet router [27], [28]. PICs were developed for packet synchronization, buffering, and switching [29] using hybrid-integrated InP, SOI, and silica waveguide chips. Optical packet buffers were designed to store packets as is done in electronic routers. The buffers used InP 2×2 optical switches to direct packets in and out of silica on silicon waveguide delays [30], but the delay line and InP to silica waveguide coupling losses limited storage to less than ten packet circulations. In the 2009 period, DARPA established the iPHOD program to address on-chip losses and to provide compact, low-cost, power-efficient, high power handling waveguide technologies for a spectrum of applications including RF microwave photonic links [31], [32], true time delay antenna beam steering using switchable optical delay lines [33], and optical gyroscopes [34] as well as packet storage. The primary goal of iPHOD was to reduce on-chip waveguide propagation loss to 0.01 dB/m over lengths of 25 m, several orders of magnitude lower than what had been achieved previously. UCSB's iPHOD effort, in collaboration with LioniX, led to a record low 0.045-dB/m loss at 1580 nm in 20-m-long waveguide spiral delay lines [35]. High aspect ratio Si_3N_4 cores with a 40-nm Si_3N_4 thick core minimized sidewall scattering. A thin layer of conformal LPCVD was deposited over the etched waveguides and planarized using chemical mechanical polishing (CMP). The thermally grown oxide upper cladding layer was wafer-bonded to the planarized LPCVD layer, to reduce absorption losses and other loss mechanisms associated with deposited oxide films [36], [35]. These waveguides supported high optical power with very small induced nonlinear optical phase shifts [37] as well as highly selective single mode transverse electric (TE) polarization propagation (>75-dB transverse magnetic loss relative to TE) [38]. However, the bonded upper cladding approach limits the types of devices and PICs as well as added fabrication complexity and lower yield. Low-loss waveguides today employ tetraethoxysilane precursor plasma-enhanced chemical vapor deposition (TEOS–PECVD) upper cladding oxide deposition, resulting in losses on the order of 0.3 dB/m [14].

C. Increasing Circuit Density and Optical Nonlinearities

The desire to make compact Si_3N_4 devices [39], [40] and increase mode confinement for efficient optical nonlinear interactions led researchers to develop thick nitride waveguides (600 nm–6.5 μm) technologies and processing techniques. The challenge was to overcome cracking that precipitated from induced stresses of thick nitride films. The MESA+ Institute for Nanotechnology using inverted slot designs for waveguides up to 900 nm in thickness [41] and Kippenberg's group at EPFL developed the photonic Damascene process [42] for core thickness up to 1.35 μm. Lipson's group advanced a two-step nitride deposition technique where mechanical isolation trenches were employed for waveguides with a core thickness of 910 nm to fabricate a resonator with Q of seven million [43]. Advances in thick nitride

waveguide technology continues to push losses continually lower.

D. From Laboratory to Foundry

Multiple commercial foundry platforms have evolved including LioniX's TriPleX [44], Ligentec's Damascene [45], IMECs BioPIX [46], and the IMB-CNM [47] processes. Commercialization of moderate optical mode confinement Si_3N_4 waveguides began in the 1980s and early 1990s with transition of research at the University of Twente, The Netherlands. Two efforts transitioned in parallel, PECVD SiO_xN_y [48], [49] and LPCVD Si_3N_4. Waveguide geometries at the time were applicable to sensing applications [50] due to the intrinsic maximum thickness of ~300 nm associated with LPCVD Si_3N_4. Technological developments in the late 1990s [39] led to the formation of LioniX in 2001 and commercialization of the TriPleX platform in 2003. The TriPleX technology uses a multilayer approach to overcome the restriction of a single-layer 300-nm-thick Si_3N_4 layers [40]. In 2010, Ligentec commercialized a waveguide geometry tailored for nonlinear optics based on the photonic Damascene process [42], a spinout technology from Kippenberg's group at EPFL. The Damascene waveguide design provides strong optical confinement with core thickness up to 6.5 μm, suitable for highly compact and nonlinear optical applications including compact Kerr-comb generation resonators [51]. Today, IMEC fabricates devices using a PECVD nitride in order to keep the process in their CMOS line, illustrating the benefits of CMOS compatible foundry processes.

III. Si_3N_4 TECHNOLOGY AND PLATFORM

Three types of waveguides are used today with variations in core geometry and fabrication process. Waveguide cross-section geometries and SEM images for the symmetric double-stripe (DS), asymmetric double-stripe (ADS) and box shape, and the buried waveguide are shown in Fig. 2. The single- and double-stripe geometries are part of the TriPleX foundry platform [13], [52] and used in the ultralow-loss waveguides developed at the University of California Santa Barbara (UCSB) [53]. The buried designs are part of the TriPleX and Photonic Damascene foundry processes. Waveguides are fabricated on an extremely flat substrate, typically single-crystal silicon, and in some applications fused silica glass substrates when transparency in the visible light region is required. The stripe waveguide geometries consist of an alternating layer stack of SiO_2 cladding layers and Si_3N_4 core layers. Further details of the fabrication processes for the TriPleX and the Damascene platforms can be found in [52] and [54].

PIC building blocks typically contain straight and curved waveguide sections with a tradeoff between waveguide propagation loss and the minimum bend radius being an important consideration. The Si_3N_4 core thickness,

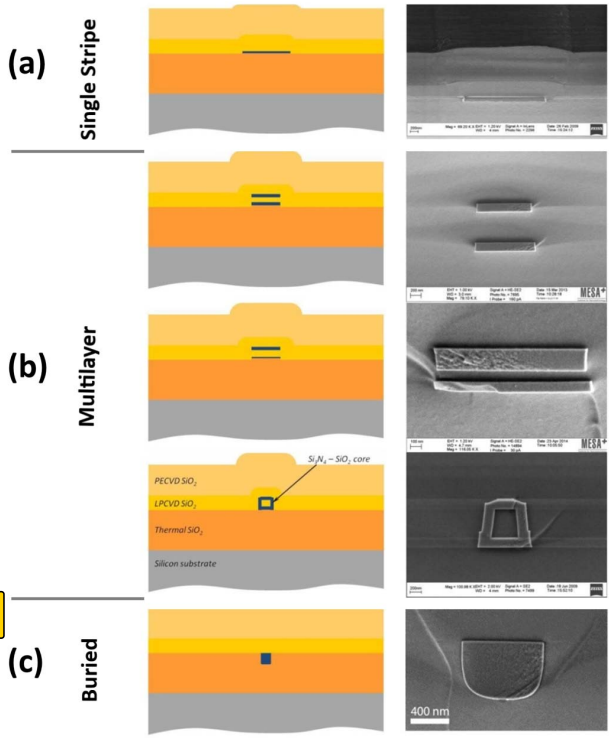

Fig. 2. *Si_3N_4 waveguide types, cross sections and SEM photographs: (a) single stripe; (b) multilayer structures comprising both double stripe (DS) and asymmetric double stripe (ADS and box shapes); and (c) buried waveguides [13].*

waveguide width, and waveguide bend radius form a design space, conveniently illustrated using the ring resonator quality factor (Q) as shown in Fig. 3(a). The waveguide loss, resonator Q, and free spectral range (FSR) vary as the core thickness is increased. Straight and large to moderate radius waveguide losses are dominated by the core sidewall scattering. As the bend radius is decreased below a critical value, bend losses dominate. It can be seen that for a fixed waveguide width a given core thickness, designing bends above the critical radius sets the lower loss as shown in Fig. 3(b). Thin cores and small bend radii are chosen when resonators with a small FSR and high Q are required, as shown on the left side of Fig. 3(a). Increasing the core thickness creates a more confined optical mode and is appropriate for designs with smaller bend radii that can accommodate larger FSRs and lower Q as shown on the far right of Fig. 3(a). Fig. 3(c) illustrates the loss contributions as a function of the core width for a 100-nm-thick core [55]. When the optical mode diameter is approximately equal to the core width the waveguide is in the high confinement regime. As the core width is decreased, the optical mode diameter grows rapidly and enters the squeezed out regime. The PIC designer can choose the loss and its sensitivity to device footprint with the appropriate core thickness by moving between bend loss limited and scattering loss limited regimes as shown in Fig. 3(d) [56].

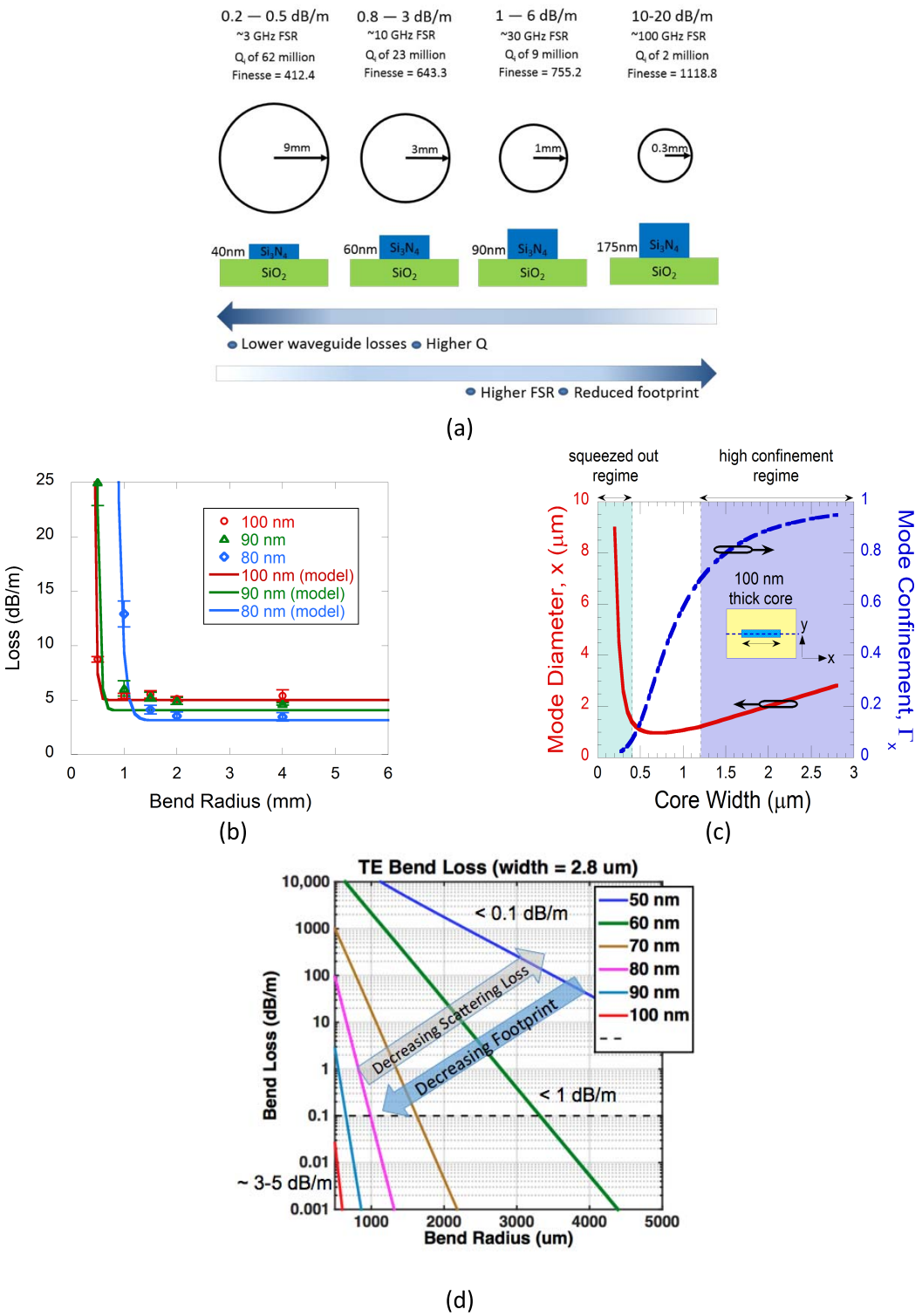

Fig. 3. ***Weakly and moderately guiding high-aspect ratio Si3N4 waveguides. (a) Tradeoffs between core thickness, loss, FSR, and minimum bend radius. Reprinted with permission from [14], ©IEEE 2018. (b) Critical bend radius for various core thicknesses. Reprinted with permission from [55], ©OSA 2011. (c) Mode confinement as a function of core width. Reprinted with permission from [55], ©OSA 2011. (d) Sensitivity to device footprint with the appropriate core thickness by moving between bend loss limited and scattering loss limited design regimes [56].***

Thinner core resonators with a bonded upper cladding layer have been used to fabricate two-mode waveguides with lower losses than their single-mode counterparts, to yield a loaded Q as high as 42 million and propagation loss of ∼0.3 dB/m [57]. Single-mode waveguide resonators have been demonstrated with Q as high

Table 1 Si_3N_4 Waveguide Types

Waveguide type	General use	References
Single stripe	Ultralow propagation losses, optimized fiber coupling	[35], [14], [57]
(Asymmetric) double stripe	Low propagation losses, tight bends, tapering to single stripe	[52], [13], [58]
Box-shape	Polarization independence	[40]
Buried waveguide	Highly confined, nonlinear	[13], [42], [41]

as 30 million and propagation loss ∼0.5 dB/m [14]. One can choose thicker core designs for more compact structures, as with a third-order filter with loaded Qs on the order of two million, propagation loss of ∼17 dB/m and a radius of ∼0.3 mm [14]. An important quantity is the mode field area (MFA), defined where the optical power has dropped to $1/e^2$ of the maximum intensity. The MFA for a 40-nm core design is on the order of 28 μm^2, whereas for the 175-nm core it is on the order of 4.5 μm^2. Large MFAs are used where low-loss and high optical power handling without inducing nonlinear phase shifts [37] is required. A summary of the different waveguide types in Si_3N_4 with their general use with example references is given in Table 1.

IV. INTEGRATION BUILDING BLOCKS AND PROCESS DESIGN KIT (PDK)

A wide variety of building blocks have been realized in the Si_3N_4 platform including bends, crossings, gain blocks, and directional couplers [52], [59]. Examples of building blocks are summarized in Table 2 and can be used to realize higher level photonic functions and circuits including spot-size converters, thermal and stress-optic actuators, and optical signal filtering and optical resonators.

As Si_3N_4 photonics has reached wafer-scale processing stability, designers can choose from guaranteed building blocks as a functional element without knowing the processing details and assemble these blocks into higher level functions and circuits. The process design kit (PDK) is a collection of (digital) files used to describe and model the fabrication process used in a variety of design tools used in designing a PIC. A PDK is created by the foundry and passed to the end user to use during the design process who in turn uses the PDK to design, simulate, draw, and verify the design. A finished design is transferred back to the foundry to produce chips. Several PDKs are available for today's Si_3N_4 foundries that are supported by a broad range of optical design software at different levels ranging from circuit design to optical wave propagation. The availability of these PDKs is a good measure that Si_3N_4 photonics has reached a mature state within multiple foundries.

V. FUNCTIONS AND APPLICATIONS

Applications range from the visible wavelength range to the mid-infrared (MIR), and span a wide variety of areas from communications, to sensing and biophotonics. In this section, we cover examples that span from the IR down through the MIR, near-infrared (NIR), and visible.

The IR range (1.0–2.3 μm) takes advantage of the transparency and low loss as well as the ability to copackage Si_3N_4 circuits with SOI and InP. Applications include lasers, optical filters, delay lines, true time delays, optical signal processors, and optical frequency comb generation. While these components have been primarily demonstrated in the IR, they can be migrated to the visible and NIR with waveguide geometry adjustments and swapping out the sources and detectors to the waveband of interest.

In the visible light (400–700 nm) and NIR (700–1000 nm) wavebands Si_3N_4 compliments the

Table 2 Si_3N_4 Building Blocks Used to Form Higher Level Photonic Functions and Circuits

Building block	Function	References
Mode converters and transition elements	Spot size converters	[52],[60]
Waveguide actuation: Thermal and piezo electric (PZT)	Thermal tuning, stress-optic tuning	[61], [62], [63], [52]
Optical filters and resonators	Single bus and double bus microring resonators (MRRs), asymmetric MZI, Bragg grating filters	[64], [14], [65], [66], [51], [52], [67], [58], [68]
Optical gain	Hybrid attached SOA, rare earth doped layers, colloidal quantum dots	[69], [70], [70], [71], [72], [73], [74], [76], [77]

capabilities of SOI photonics. Applications include sensing and spectroscopy, atomic physics, quantum communication and computation, microscopy, biophotonics, and astronomy. Portable and remote sensing applications can leverage chip-scale integration of chemical and biological sensors. Other visible and NIR applications include LIDAR, free-space communications, laser-based display and vision applications. Two areas that have received increasing attention are biophotonic sensing, spectroscopic sensing, and chemical sensing. Biophotonic sensing is used to measure and image optical processes in biological systems including cells and tissue. Spectroscopic sensing [78] allows measurements to be made without specifying the types of cells and without labeling the cells so that living cells can be characterized [79]. Chemical sensing including detection of label-free gases in ambient atmosphere, such as CO_2 and volatile organic compounds. Si_3N_4 photonics promises to bring these applications to the "lab-on-a-chip" level [80].

A. Lasers

Si_3N_4 platform offers multiple approaches to high-performance lasers on-chip, with emission from the visible to IR possible through the wide wavelength transparency and a suitable pump source or gain material. Si_3N_4 lasers fall into three categories, external cavity resonators with a semiconductor gain block hybrid attached or bonded to the Si_3N_4 PIC, optically pumped rare earth ions or quantum dots with the gain material incorporated into the Si_3N_4 guiding region, and scattering processes such as Brillouin and Raman. The quality of light, measured in terms of coherence (or linewidth) and relative intensity noise (RIN) as well as other parameters including output power, wavelength, wavelength tuning range drive, and power consumption drive the choice of design. Low-loss Si_3N_4 cavities give the laser designer the ability to store many photons in extremely high Q resonators or long on-chip cavities.

External cavity lasers traditionally combine semiconductor optical amplifiers (SOAs) gain blocks with external high Q discrete components such as fiber Bragg gratings (FBGs) to realize tunable sources with linewidths as low as 15-Hz fundamental linewidth [81]. This level of performance has the potential to move on-chip using Si_3N_4 high Q resonators or long side-wall etched gratings. A compact hybrid laser with 13-kHz integral linewidth was demonstrated with an InP gain block coupled to a high Q Si_3N_4 microring resonator (MRR) external laser mirror [82]. A variation of this approach, as shown in Fig. 4, incorporates a long photon lifetime Si_3N_4 MRR tuning section with tunable wavelength output and fundamental linewidth less than 300 Hz [83].

The performance of erbium doped fiber lasers and amplifiers can be moved on-chip by combing the low loss of Si_3N_4 waveguides with long, low kappa sidewall grating filters as mirrors and erbium ions as the gain

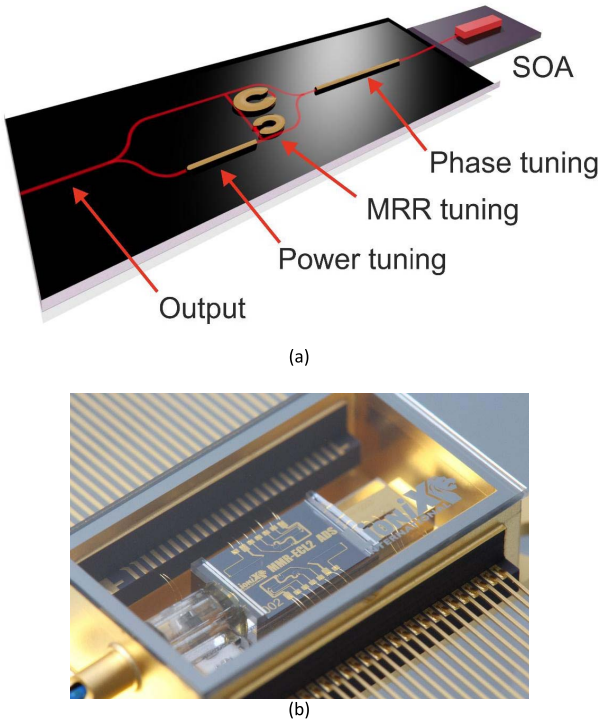

Fig. 4. ***An InP–Si_3N_4 hybrid external cavity laser. (a) Principle components: InP-based gain section (SOA) connected to tunable mirror in Si_3N_4 platform. (b) Assembled device as seen in [84].***

medium. Compared to semiconductor-based hybrid Si_3N_4 lasers, rare-earth-ion-doped lasers exhibit relatively narrower lasing linewidths (~3-kHz integral), higher degrees of temperature stability, and lower laser noise as with their fiber counterparts [85]. Low linewidth WDM distributed Bragg reflector (DBR) and distributed feedback (DFB) laser arrays are fabricated using an active layer of cosputtered erbium ions (Er^{3+}) and aluminum oxide (Al_2O_3:Er^{3+}) on sidewall etched Si_3N_4 waveguides [71]–[73]. These lasers exhibit stable high-temperature operation typical of erbium-doped lasers, up to 400 °C, with minimal performance degradation [86]. Such devices require only a single lithography and etch step of the nitride core to define the Bragg mirrors as shown in the SEM images in Fig. 5(a). Simple fabrication processing of WDM laser arrays, using CMOS deep UV (DUV) lithography is used to fabricate WDM lasers arrays by adjusting the grating period Λ [Fig. 5(b)]. Optical spectrum traces in Fig. 5(c) show emission over a wide wavelength range with well-defined wavelengths.

Microlasers with emission at 630 nm use colloidal quantum dots formed between two Si_3N_4 resonator layers and coupled to a Si_3N_4 waveguide [77]. This microdisc laser consists of a Si_3N_4 microdisc with a colloidal quantum dot layered on a SiO_2 on silicon lower cladding. The microdisc is then is vertically coupled to a Si_3N_4 waveguide bus and optically pumped as illustrated in Fig. 6(a). The emission photoluminescence (PL) below and above threshold

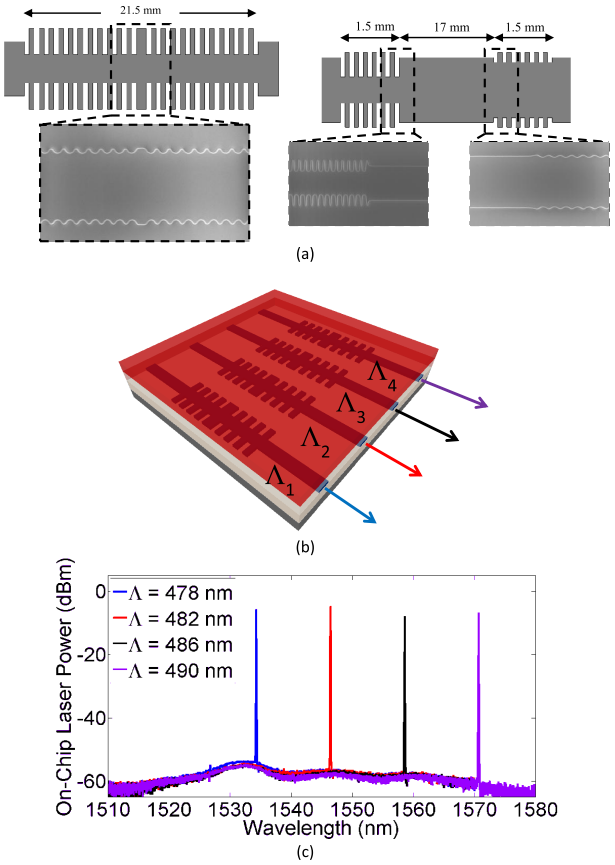

Fig. 5. ***Erbium-doped aluminum oxide (Al_2O_3:Er3+) Si_3N_4 waveguide lasers. (a) SEM images of sidewall etched DBR and DFB waveguide cores. Reprinted with permission from [72], ©OSA 2014. (b) Monolithic WDM laser array from [75]. (c) Optical spectrum output. Reprinted with permission from [72], ©OSA 2014.***

[Fig. 6(b)] and optical pump power versus laser bus output power demonstrates lasing threshold [Fig. 6(c)].

B. Optical Filters

Optical filters are used to select frequencies transmitted on an optical fiber, shape the spectral or temporal contents of transmitted and received signals, optimize optical signal-to-noise ratio (OSNR), and perform signal processing functions on digital and analog optical signals. Microwave photonics (MWPs) involves the transmission of RF (∼300 kHz–300 GHz) and microwave (∼300 MHz–300 GHz) signals over optical fiber and free space optics [31], [87]. MWP devices and systems face unique challenges inherent to transmission of high fidelity analog signals including linearity, OSNR, and power handling [88]. Integrated microwave photonics (IMWPs) [89] is an area of extreme interest due to the need drive down cost and weight while maintaining high performance for applications like next-generation radio over fiber and phased antenna arrays for next-generation 5G mobile networks.

A widely used filter design is the coupled-resonator optical waveguide (CROW) structure where light propagates via chains of weakly coupled high-Q optical cavities [90]. CROW structures can be used for frequency filtering, light transmission, optical delay lines, and optical nonlinear interactions. The first CROW filter in a Si_3N_4-like waveguide was demonstrated in SiO_xN_y waveguides [91]. A polarization-independent extinction ratio of 15 dB was achieved with 100- and 50-GHz FSR designs, an optical bandwidth of 7.4-GHz bandwidth, and a 4.4-dB insertion loss. The three-resonator low-loss Si_3N_4 bus-coupled CROW filter, illustrated in Fig. 7(a), was fabricated using low-loss 175-nm-thick core and 600-μm-diameter resonators [14]. This third-order filter demonstrated an ultrahigh 80-dB extinction ratio (ER) with low insertion loss (<1.3 dB) and a flat passband [Fig. 7(b)]. The filter center frequency was tuned over the full 48-GHz FSR [Fig. 7(c)] using thermal tuning elements located in each of the three rings. A photomicrograph of the fabricated device is shown in Fig. 7(d). Filters with this level of ER and filter shape performance are used in a wide range of application including pump-signal separation in Brillouin, four-wave mixing (FWM), second-order nonlinear generation, spectroscopy, and receiver channelization in RF photonics.

Filter channelization is used in RF photonic and WDM optical communications to tune individual channel bandwidths in addition to center frequency tuning, adding to circuit complexity and device and waveguide loss and linearity requirements. Channelization is used to set the bandwidth of transponders, to separate channels

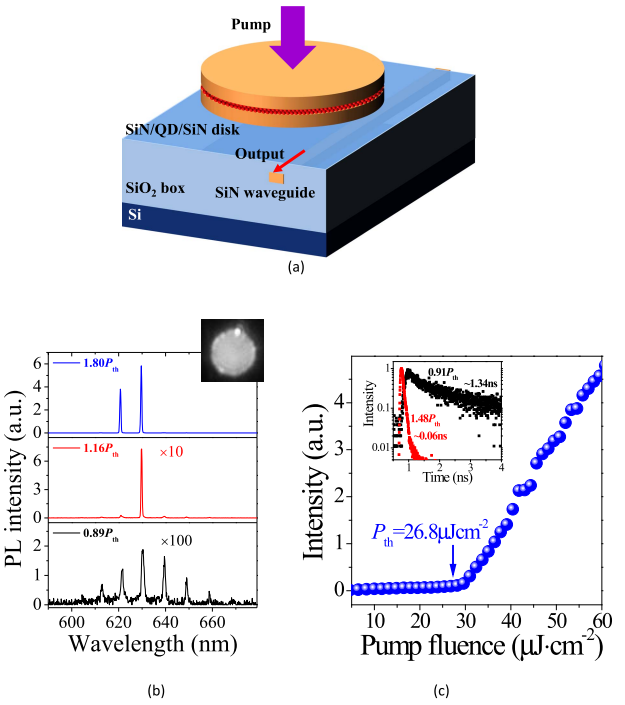

Fig. 6. ***Optically pumped visible emission colloidal quantum dot Si_3N_4 laser. (a) Laser geometry. (b) Photoluminescence (PL) emission spectrum below and above lasing with 630-nm lasing observed. (c) Pump power versus PL demonstrating lasing threshold. Reprinted with permission from [77], ©OSA 2016.***

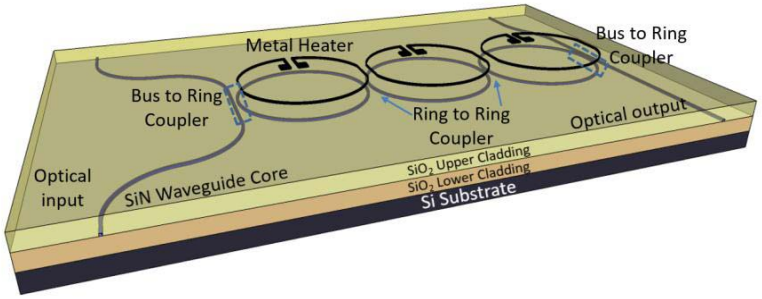

(a)

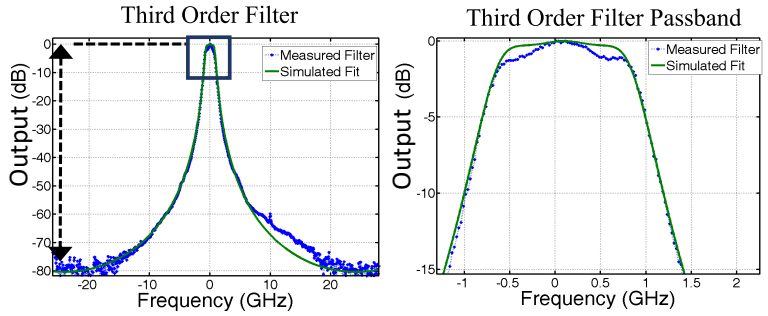

(b)

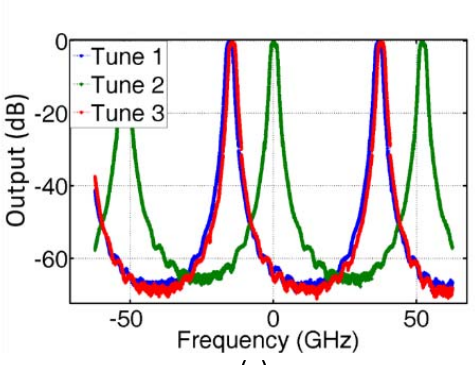

(c)

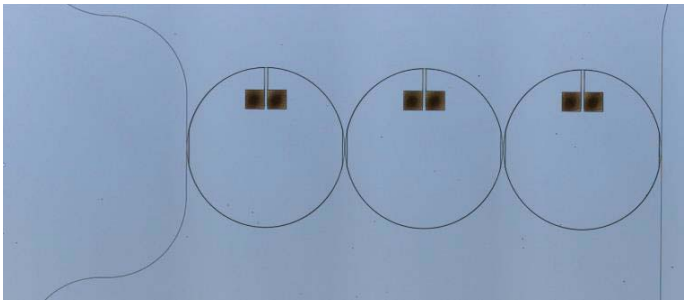

(d)

Fig. 7. ***(a) Schematic of low-loss third-order tunable CROW filter. (b) Measured 80-dB extinction ratio. (c) Filter tuning across a full FSR. (d) Photomicrograph of fabricated filter. Reprinted with permission from [14], ©OSA 2018.***

prior to amplification, and to control adjacent channel interference. Si_3N_4, with its low-loss elements, brings a solution to large, complex, tunable, for chip-scale channelizers that has been difficult to fabricate in other technologies. A CROW-based bandpass filter fabricated in the TriPleX platform is capable of selecting a channel in a frequency-division subcarrier satellite communication system [92]. The basic functional circuit is shown in

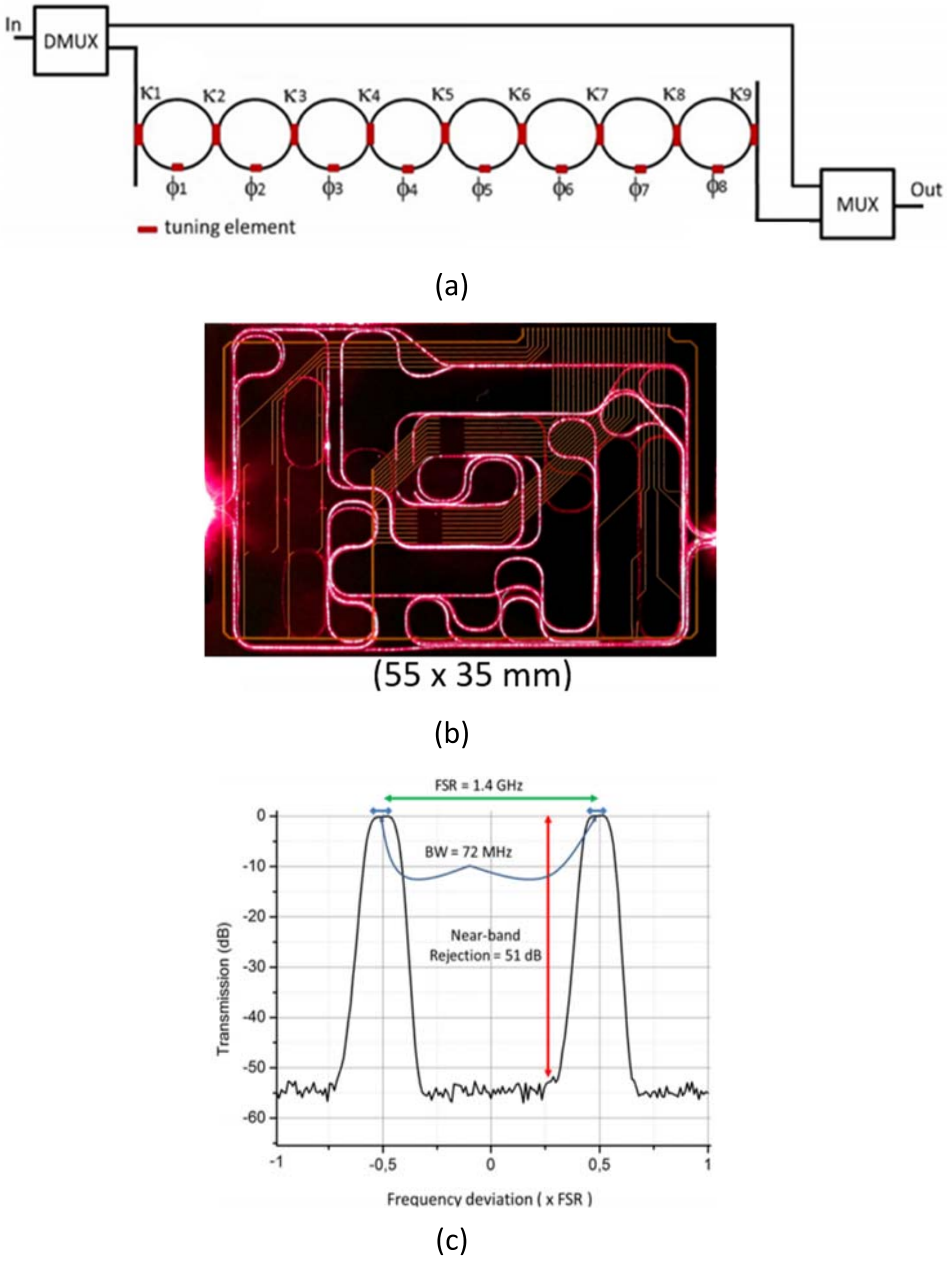

Fig. 8. ***Optical channelizer for subcarrier satellite communication system. (a) Functional circuit design. (b) Three-dimensional chip layout. (c) Photomicrograph under red laser illumination. (d) Measured channelizer transmission output power. Reprinted with permission from [52], ©IEEE 2018.***

Fig. 8(a). Thermally tuned phase shifters at each resonator are combined with thermally tuned power couplers to enable arbitrary filter programming. Center frequency tuning over a full FSR in addition to tunable channel bandwidth as small as tens of megahertz can be performed. For example, a K_u-band input multiplexer (IMUX) requires a channel bandwidth ranging from 27 to 95 MHz for the frequency band from 10.7 to 12.75 GHz. Fig. 8(b) shows a 3-D layout of eighth-order coupled ring resonator network, with an FSR of 1.4 GHz, that comprises an optical carrier-sideband demultiplexer and a multiplexer with a highly frequency-selective optical filter in between [93]. A photomicrograph of the actual chip and experimental power transmission with 72-MHz passband for two channels are shown in Fig. 8(c) and (d).

A generalizable programmable RF filter network can be fabricated using low-loss tunable filter arrays, enabling multiple dynamically configurable complex filter functions on the same chip. Arrays of Si_3N_4 programmable Mach–Zehnder (MZ) couplers can be interconnected to implement a wide class of filter types (e.g., FIR and IIR) [94]. The 2-D lattice mesh network of interconnected MZ couplers, shown in Fig. 9(a), uses thermal phase tuning elements to configure each MZ coupler as a 2×2 coupler

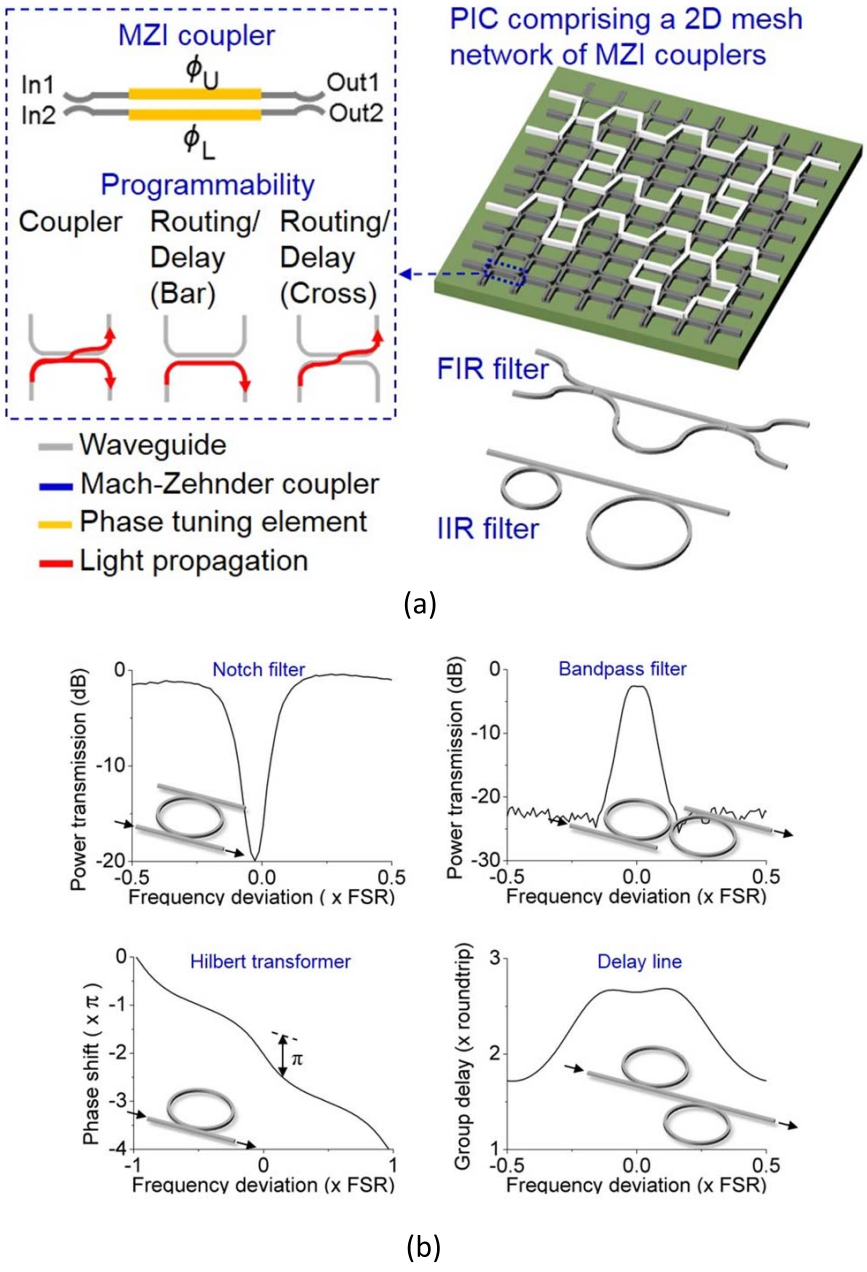

Fig. 9. ***(a) Programmable complex filter structures based on 2-D arrays of interconnected Si_3N_4 ring bus resonator filters and tunable MZ couplers. (b) Examples of programmable filter functions realized by programming two cells of the array into the associate configurations. Reprinted with permission from [94], ©OSA 2015.***

or an optical switch. Each MZ element simultaneously controls the optical amplitude and phase of its optical output. The range of circuit parameters (amplitude and phase of each optical path in the circuit) can realize multiple simultaneous programmable filter functions on the same chip, e.g., notch and bandpass filters, Hilbert transforms, and tunable delay lines, as shown in Fig. 9(b).

C. Delay Lines, True Time Delays, and Optical Signal Processors

Optical delay lines are desirable for a wide variety of applications including RF and digital filtering, optical beam forming, optical signal processing, information coding, digital data storage and synchronizers, and pulse shaping, and offer the potential for large power savings over digital electronic counterparts. Two different types of delay lines, resonant and nonresonant, are used standalone or in combination. Nonresonant delays are used for RF and analog functions like transversal and FIR filters, IIR filters, and other discrete time signal processors [95]. Discrete delay lines are applicable for feedforward structures like transversal and lattice filters, and in combination with optical switches as recirculating delays and storage elements. Broadband Si_3N_4 delays provide discrete, medium to large

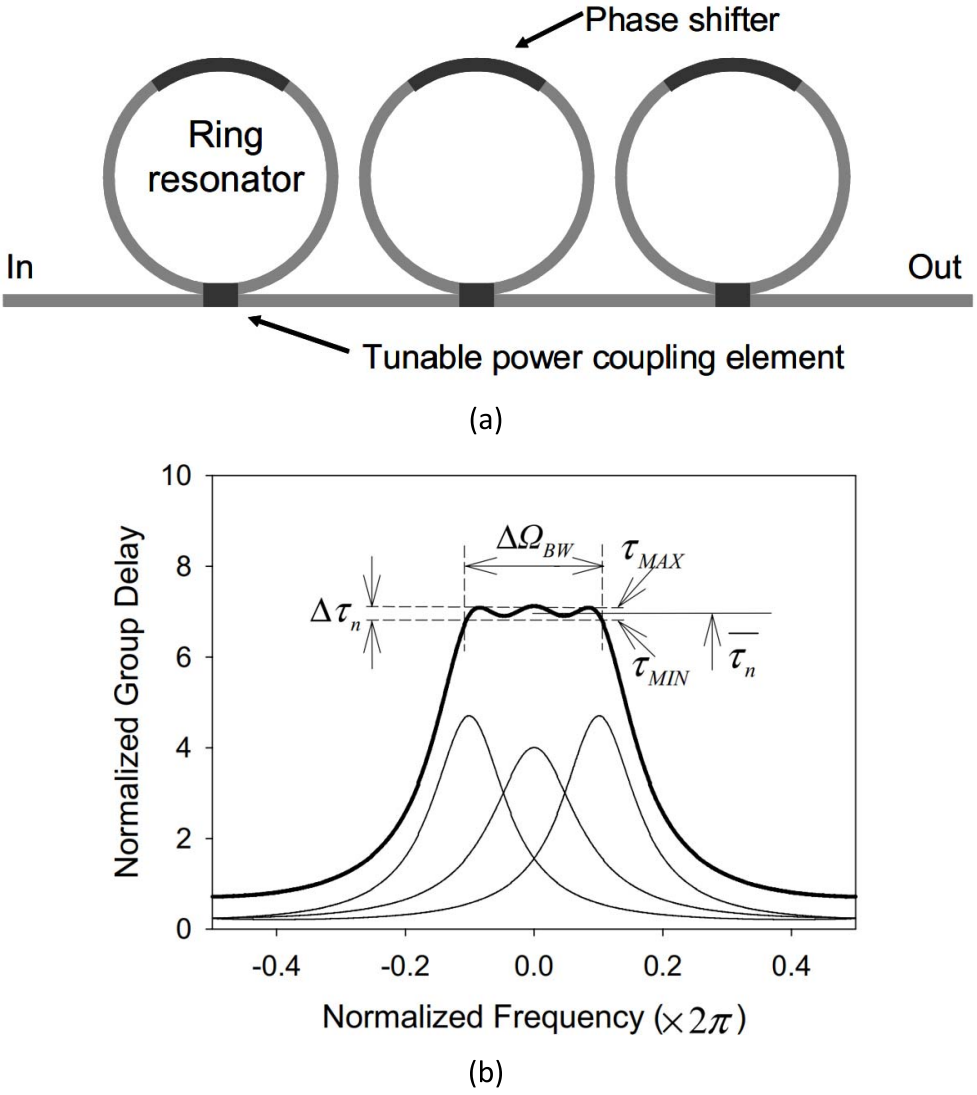

Fig. 10. *(a) Schematic layout of a three-stage ring resonator filter. (b) Calculated normalized group delay response. The bold line represents the sum (three-stage response) of the thin lines (single-stage responses). [96]*

delays, up to 250 ns on a single chip (tens of meters in length). Resonant delay lines are more compact than their nonresonant counterpart, and are continuously tunable over a fine to medium delay range (e.g., picoseconds to order of a nanosecond). However, the resonance used for delay typically supports only narrowband signals and the resonance must be tightly controlled. Optical ring resonator (ORR)-based delays [96] can be tuned by adjusting the bus to ring coupling ratio as shown in Fig. 10(a). These all-pass structures typically tradeoff the maximum amount of delay with the signal bandwidth. A simulation of group delay [Fig. 10(b)] shows a maximum delay of 1.2 ns for a signal with 500-MHz bandwidth.

Nonresonant Si_3N_4 waveguides provide about 12.5 ns per meter delay. Delay lines up to 25 m in length with 250-ns delay are fabricated on a single-layer chip using coil (spiral) configurations. Low-loss coils are fabricated using a 40-nm core and 10-mm minimum bend radius on a large area (2 cm $\times$ 2 cm) chip [97]. The large area and uniformity of processing requires techniques such as large area deep UV (DUV) lithography. Single-layer coil designs utilize multiple turns and 90° crossovers to allow input and output waveguide access. A single-layer 3-m coil with 25 turns and 50 crossings with measured 0.78-dB/m waveguide loss and 0.0156-dB/crossing loss [97] illuminated with red laser light is shown in Fig. 11(a).

Optical beam forming networks (OBFNs) for phased-array antennas is another high impact application for Si_3N_4 PICs. These systems require broad instantaneous bandwidth, continuous amplitude, and array element delay tunability, scalable to a large number of element arrays. Low propagation loss combined with high linear

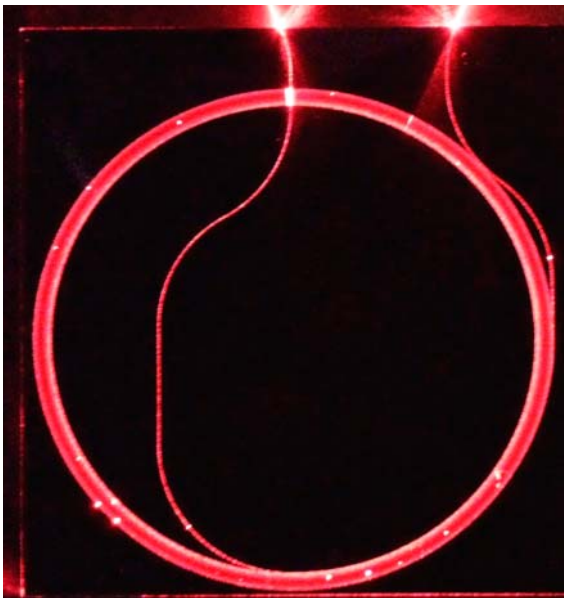

Fig. 11. *Single-layer multiple turn coil that use very low-loss 90° crossings to allow access to input and output. Shown is a red light illuminated large area 3-m coil with 25 turns and 50 crossings. Reprinted with permission from [97], ©IEEE 2017.*

power handling is essential for IMWP OBFN solutions [98]. An example chip uses resonant Si_3N_4 ORRs as continuous tunable delay elements for a phased array antenna system for mobile broadband satellite communications with 16 inputs, a 4.5-GHz optical bandwidth, and a maximum delay of 290 ps [58]. This level of performance translates to the functional equivalent of a 16×1 binary-tree combining circuit inserted symmetrically with a total of 40 ORR-based delay lines, an optical sideband filter (OSBF) using an asymmetric MZI with two ORRs, and an optical carrier reinsertion coupler. A schematic of the beam former architecture and a chip layout mask are shown in Fig. 12(a) and (b).

Larger true time delays for phased array radar and other RF applications can be fabricated using nonresonant delay lines combined with optical switches [99]. The 4-bit tunable delay layout and a photograph of a red laser illuminated fabricated chip are shown in Fig. 13. Experimental temporal delays up to 12.35 ns with resolution of 0.85 ns were demonstrated, with a total of 2.407 m of propagation length.

A Si_3N_4 programmable optical lattice filter leverages the ability to fabricate many stages of low-loss discrete delays with tunable optical couplers, providing a low-power, low-cost alternative to high-bandwidth digital processing. A programmable tenth-order lattice filter with cascaded asymmetric MZIs (aMZIs) can be designed with an FSR matched to the WDM channel spacing, allowing dispersion compensation for multiple optical channels simultaneously [100], [101]. The lattice filter was realized using 21 cascaded aMZIs to realize a ten-stage programmable tenth-order lattice filter [Fig. 14(a)]. The aMZIs are thermally tuned in one arm of each 2×2 directional coupler. The time delays are chosen to be an integer multiple of the unit delay ΔL, making the filter discrete in the time domain and periodic in the frequency domain. The frequency periodicity is chosen to be the channel spacing in a WDM transmission system. This filter can simultaneously dispersion compensate multiple WDM channels at the same time, which combined with the low loss has advantages over high loss bulky dispersion compensating fiber (DCF) and power savings over digital signal processor (DSP) based [102]. The fabricated chip has a footprint of 2.23 cm^2 and utilized delays $\Delta L = 2$ mm [Fig. 14(b)] with the capability to continuously tune dispersion from -500 to 500 ps/nm for each channel on a 100-GHz grid with a single device. The transmission and group delay tuning curves for one channel are shown in Fig. 14(c).

D. Optical Frequency Comb Generation

Si_3N_4 optical frequency comb generators provide a single source of multiple well-defined equally spaced frequencies over extremely broad ranges (e.g., 70 THz) in the visible, NIR, and MIR wavebands. Comb generators are an attractive solution to replace large arrays of power hungry WDM lasers for high capacity fiber communications systems. Other applications include spectroscopy frequency generation, laser sensing, waveform synthesis, optical metrology, and optical frequency referencing. Early comb generators were constructed using discrete component mode-locked lasers (MLLs) and feedback stabilization [103]. Chip-scale comb designs include mode-locked lasers (MLLs) [104], high-speed phase modulators [105], gain switched comb sources (GSCS) [106], and microresonator Kerr frequency combs [51], [107]. Si_3N_4 Kerr microresonator combs have the advantage of a wide comb spacing (>100 GHz) that is difficult to achieve with other comb techniques. Kerr microresonators exhibit extremely uniform mode spacing and high stability. Early comb generators were fabricated in silicon [108] and silica [51]. These concepts were migrated to Si_3N_4 resonator technology enabling comb generation in the visible and near to mid-IR. The absence of nonlinear losses mechanisms (like two-photon absorption in silicon) for efficient Kerr-driven FWM in the visible, NIR, and MIR make this a powerful platform for expansion of applications beyond the far IR. Given the flexibility in Si_3N_4 photonics to design a wide range of low-loss waveguide resonators with different FSRs, the comb generator line spacing can be optimized for a given application. Of particular interest is the dissipative Kerr soliton (DKS) microresonator comb generator [109] that balances nonlinear four-wave mixing parametric gain, cavity loss, and dispersion to generate continuously circulating pulses in an optical microresonator that yield a frequency comb output as illustrated in Fig. 15(a). The output of a Si_3N_4 240-μm radius ring resonator, shown in Fig. 15(b), generates a 3-dB bandwidth of 6 THz,

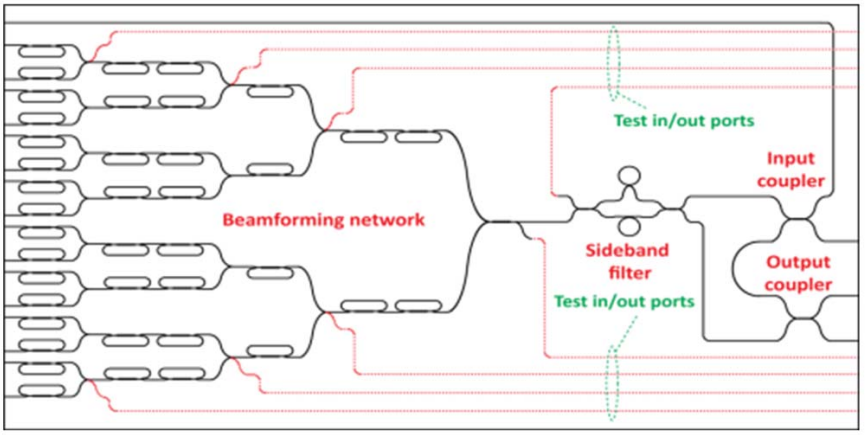

(a)

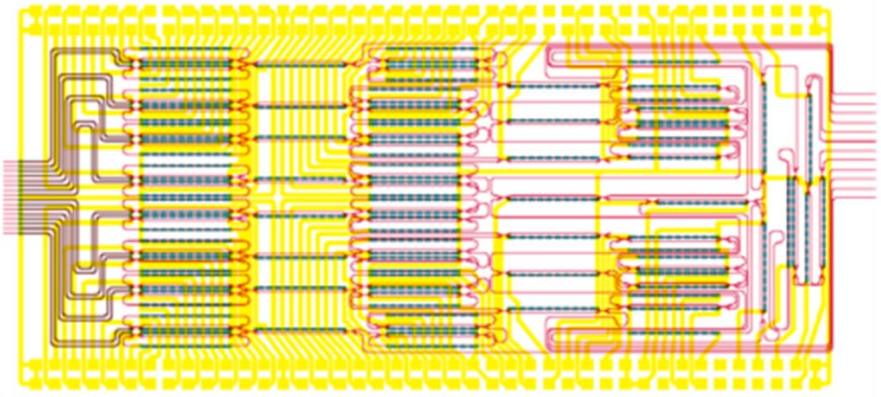

(b)

Fig. 12. *Optical beam forming networks PIC. (a) Schematic of the 16 × 1 OBFN chip. (b) Chip mask layout. Reprinted with permission from [98], ©OSA 2013.*

covering the full telecommunications C- and L-band [110]. This comb generator was used to demonstrate a parallel WDM coherent fiber communications link operating at tens of terabits per second [111]. A conceptual illustration of a terabit per second chip-scale transmitter is shown in Fig. 15(c). More in-depth reviews and experimental comparison of integrated optical comb techniques are provided in [112] and [107].

E. Supercontinuum Generation

Ultrabroadband optical spectra can be obtained by supercontinuum generation (SCG) and is used in

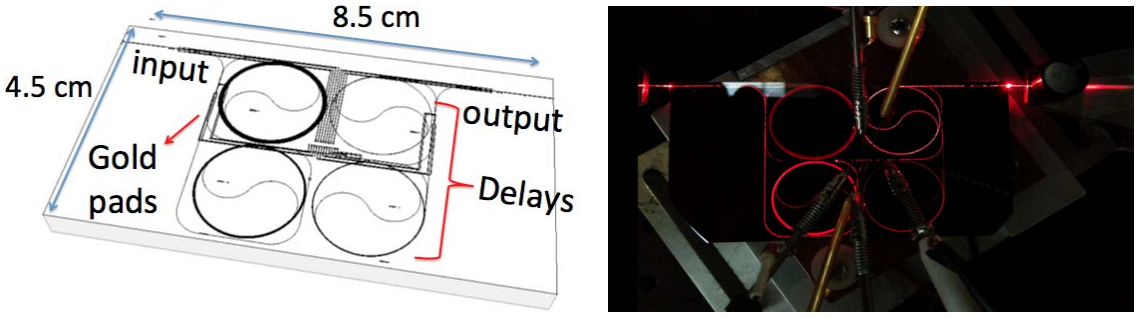

Fig. 13. *A 4-bit tunable delay for broadband phased array antenna applications with resolution of 0.85 ns and total delay of 12.35 ns. Reprinted with permission from [99], ©IEEE 2013.*

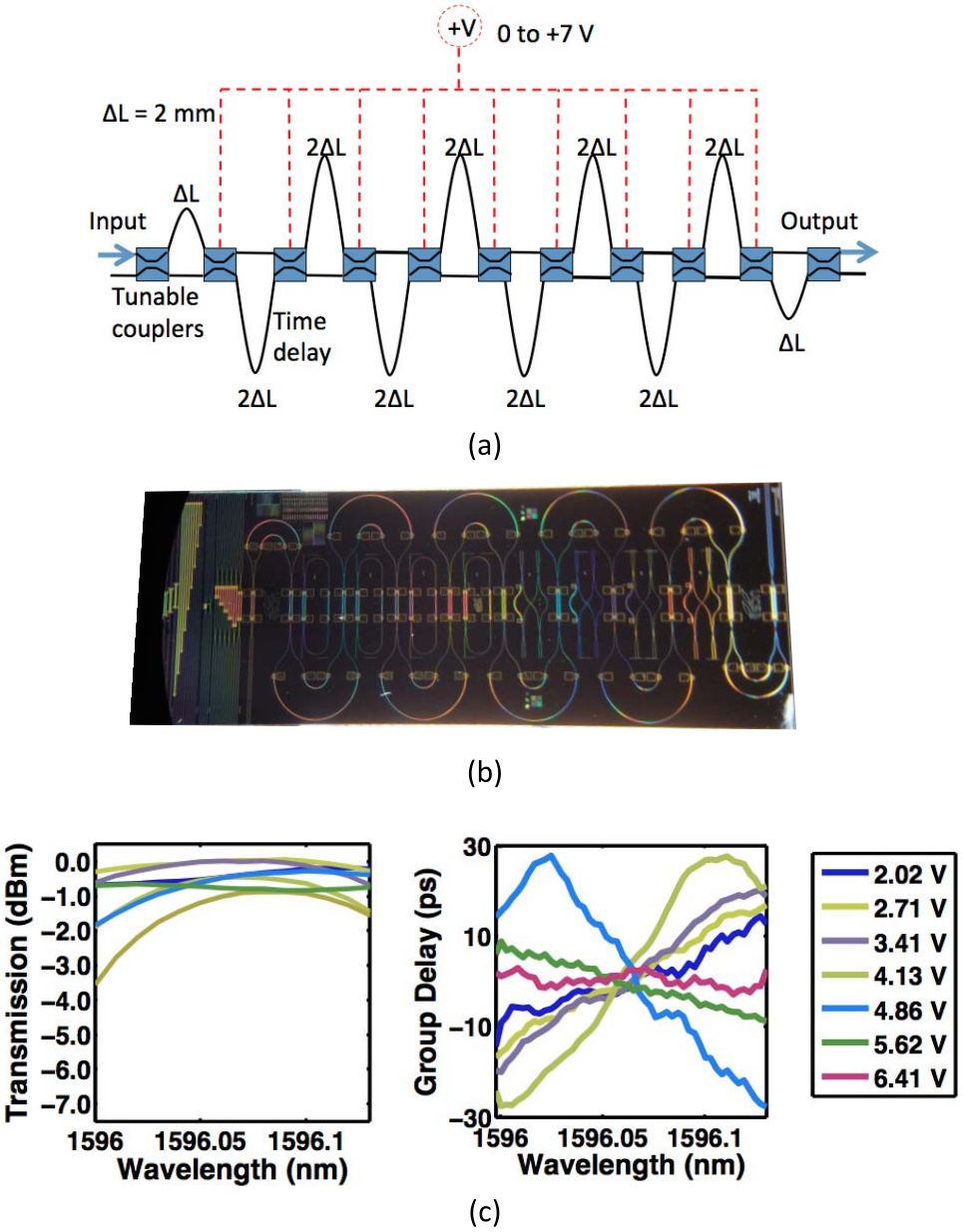

Fig. 14. *(a) Programmable tenth-order lattice filter configuration with 21 cascaded tunable aMZIs. (b) Photograph of fabricated chip. (c) Transmission and group delay tuning curves for one channel. Reprinted with permission from [101] ©OSA 2016.*

applications such as biophotonics, optical coherence tomography, coherent spectroscopy, and frequency metrology. Of particular interest is extending SCG into the visible range. Early work on SCG in integrated Si_3N_4 waveguides used ultrashort pulses at 1.3 μm in a 4.3-cm-long waveguide [113] and 1.5 μm in a 1.4-cm-long waveguide [114] to generate at the edge of the visible range, 665–2025 nm and 70–2400 nm, respectively. Extension of SCG generation into the visible toward the blue range (488–978 nm) was later achieved using a 1-cm-long Si_3N_4 photonic waveguide with an octave spanning output spectral bandwidth of 310 THz [115]. To obtain shorter wavelength supercontinua on a chip a shorter wavelength pump is required as well as suitable dispersion for the shorter pump wavelength. This principle was used to demonstrate the widest SCG output at the time [41], extending from the visible (470 nm) to the IR spectral range (2130 nm). The output comprises a spectral bandwidth wider than 495 THz as shown in the spectrum and spectrometer output in Fig. 16(a) and (b). The ability to perform energy-efficient octave spanning SCG in compact Si_3N_4 waveguides has also enabled precision stabilized low-noise frequency combs, discussed in the previous section, that are self-referenced and alleviate the need for extremely stable optical references [116], [117]. A record two-octave spanning

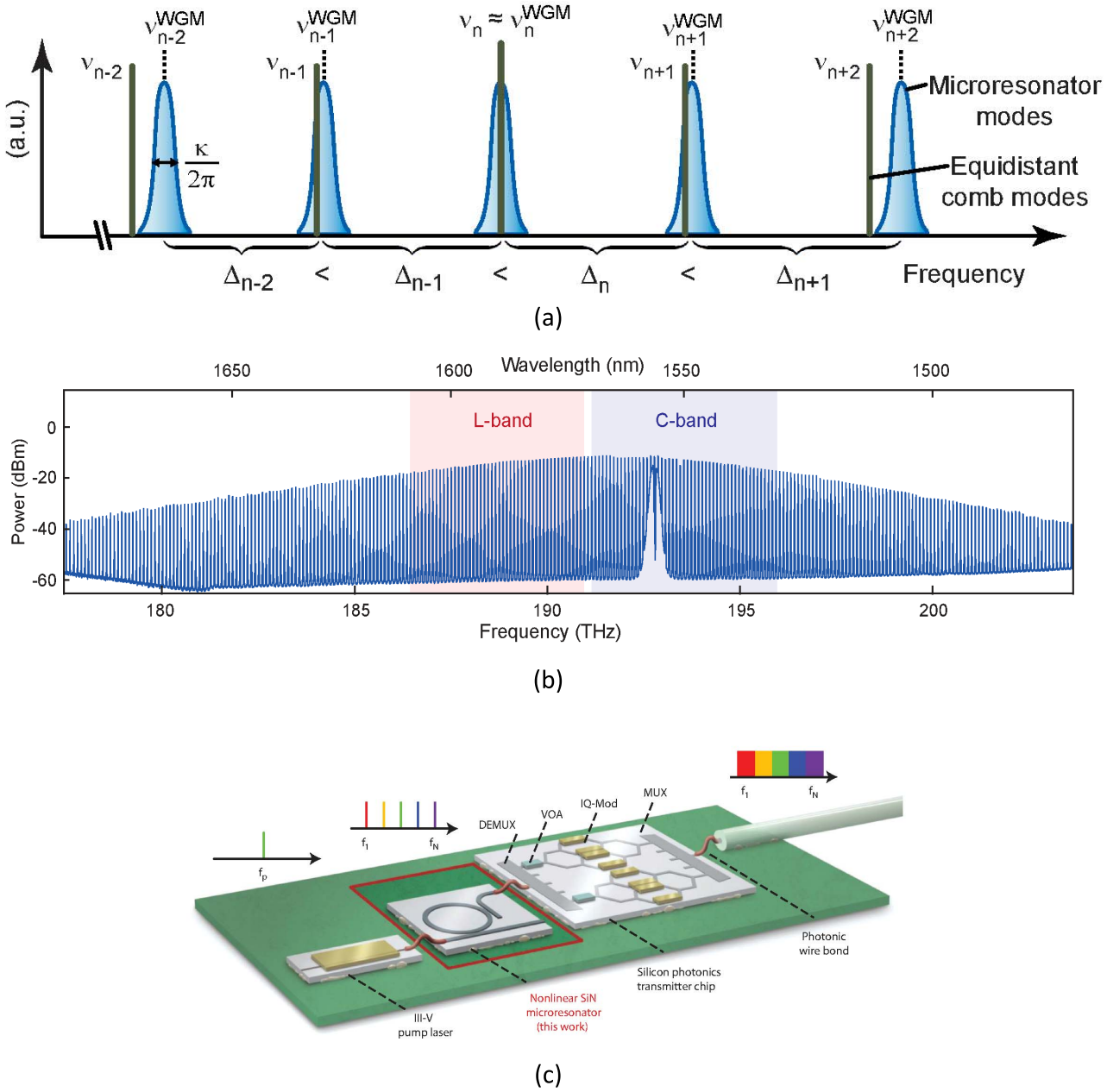

Fig. 15. *(a) Principle of resonator-based comb generation based on degenerate and cascaded nondegenerate FWM. Reprinted with permission from [107], ©AAAS 2011. (b) Stable, uniform, highly coherent output with 3-dB BW of 6 THz and C- and L-band coverage. Reprinted by permission from Macmillan Publishers Ltd.: Nature 5(46), 274-9 (2017) [110]. (c) Artist rendition of terabit per second transmitter with Si_3N_4 comb generator and silicon photonic multichannel WDM modulator. Reprinted by permission from Macmillan Publishers Ltd.: Nat. Phot. 8, 375-80 (2014) [111].*

SCG used stoichiometric Si_3N_4 waveguides pumped at telecom wavelengths [118] produced extended SCG generation from the visible (∼526 nm) to the MIR ($> 2.6\ \mu$m).

F. Spectroscopic Sensing and Lab on a Chip

For portable spectrographic applications, moving today's box sized equipment to a "lab on a chip" is essential. Building blocks that need to be combined on chip include an optical source, a sample sensor, and spectrally selective optical elements and photodetectors. Spectrographic systems use absorption, emission, or scattering methods (e.g., Raman) to detect the presence of and analyze information contained in biological and chemical samples.

With absorption spectroscopy, a broadband light source or wavelength tunable laser is used to probe the sample and the transmitted spectrum is analyzed using photodetectors in combination with a dispersive optical element [e.g., a prism, an arrayed waveguide

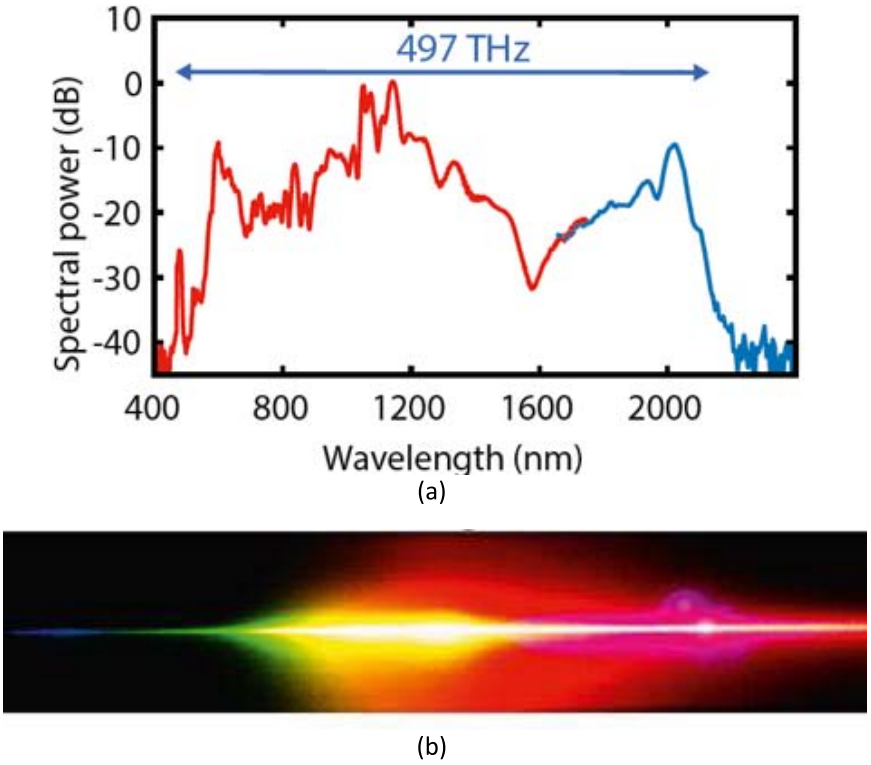

Fig. 16. *Supercontinuum spectrum generated in a 5.5-mm-long Si_3N_4 waveguide. (a) The optical spectrum extends more than 495 THz from 470 to 2130 nm. (b) Photograph of imaged spectral output. Reprinted with permission from [41], ©OSA 2015.*

grating multiplexer (AWG) or parallel or tunable optical filters]. Coverage over the 400–1700-nm wavelength span requires three AWG designs operating in the visible (VIS) (400–700 nm), NIR (700–1000 nm), and MIR (1000–1700 nm) wavebands [119], [120]. An image of the VIS AWG output with a broadband supercontinuum laser fiber coupled to the input is shown in Fig. 17.

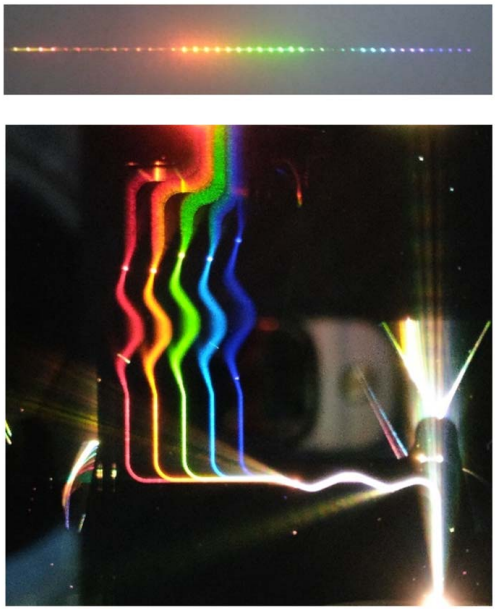

Fig. 17. *Si_3N_4 photonic spectrometer for tissue sensing application. An imaged output of the visible wavelength AWG is shown. Reprinted with permission from [119], ©IEEE 2017.*

Many applications require the analysis of fluidic and gas-sensing requiring an interaction between the material to be measured and optical waveguides. Also known as micro–optical fluidic systems (MOFSs), these chips utilize light to control the fluid flow or fluid flow to guide light, at the micrometer scale and are also used to analyze and sort particles and cells [121]. The interaction between light and the material to be measured occurs through either evanescent field or refractive index sensing. Evanescent sensing involves local removal of the waveguide top cladding such that the optical field is in contact with the environment. Early work in Si_3N_4 [24] and more recently [80], [122] are examples of this approach. Refractive index-based sensing is an alternative approach that involves etching a slot or channel through the waveguide core to act as the fluidic sensing channel that carrier the material. Examples include a Si_3N_4 slot waveguide [123], slotted bus-coupled ring resonator [124], and a full trench used to both trap and analyze particles with light [6]. Sensing using optical interferometric or resonator structures, like bus-coupled ring resonators or MZIs, enhances the sensor sensitivity with a tradeoff in reduced measurement bandwidth.

An example of an evanescent optofluidic sensor is shown schematically in Fig. 18(a) where the SiO_2 optical waveguide cladding is etched down to the Si_3N_4 core.

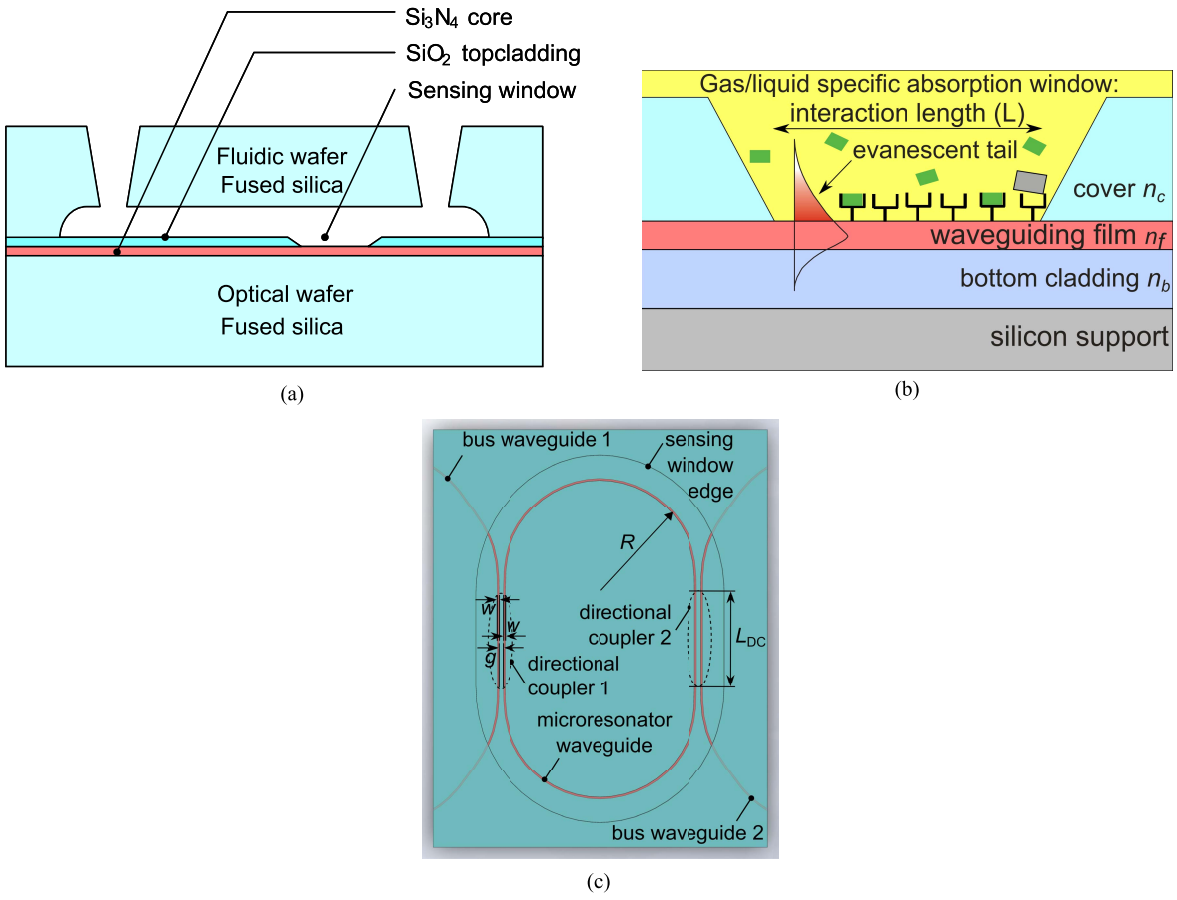

Fig. 18. ***(a) Schematic of a cross-sectional view of an optical signal propagating through an optical planar waveguide [13]. (b) The optical evanescent tail interacting with a sensing window [13]. (c) Integration of evanescent optofluidic sensor into a Si_3N_4 bus-coupled ring resonator [125].***

A fluidic channel is formed over a sensing window with a secondary fluidic cover wafer bonded on top. The gas or liquid is passed by the waveguide sample window and interacts with the evanescent tail of the optical mode, which is mostly confined in the Si_3N_4 core [Fig. 18(b)]. Fabrication of the evanescent optofluidic sensor window (shown in dotted oval region) into a Si_3N_4 bus-coupled ring resonator is shown in Fig. 18(c).

In Raman spectroscopy, laser light incident on a sample is scattered and shifted in frequency by energy related to molecular vibrations, yielding a "fingerprint" of the sample [126]. One of the challenges with Raman spectroscopy is to build up a sufficient signal-to-noise ratio (SNR) in the Raman spectrum. Techniques like Raman tweezers spectroscopy have been developed to address this issue by holding the particle during analysis. In Raman tweezers spectroscopy, the laser probe light also serves to immobilize the particle by optical trapping. An integrated photonic Si_3N_4 PIC for Raman tweezers spectroscopy was fabricated using a dual-waveguide configuration operating at $\lambda = 785$ nm [6]. The waveguide is the TripleX box waveguide shown in Fig. 19(a) and (b) and the guided optical mode in Fig. 19(c). The device is fabricated as an assembly of a waveguide, a 50/50 Y-junction and a loop [Fig. 19(d)]. To create the trapping geometry, a gap [Fig. 19(e)] is opened in the loop by dry etching successively through the upper cladding (SiO_2) and the waveguide and the lower cladding (SiO_2). In this way, an integrated fluidic channel and two faceted waveguides, from which counterpropagating beams are launched into the channel, are formed in a single step. Trapping results from a force directed transverse and a parallel to the optical beams, together determining the particle's position in the trap. Integration of the optical source using heterogeneously integrated silicon photonic/III–V lasers and wavelength arrayed waveguide grating spectrometers [127] can be achieved in the Si_3N_4 platform for operation in the MIR, NIR, and visible.

G. Microscopy and Imaging

Combining multiple visible laser lines is required for applications such as microscopy and display and projection. Combination of two to eight laser lines is used in fluorescence detection to image or distinguish structures with subwavelength dimensions. For example, in super resolution microscopy, high end lasers are used at the typical

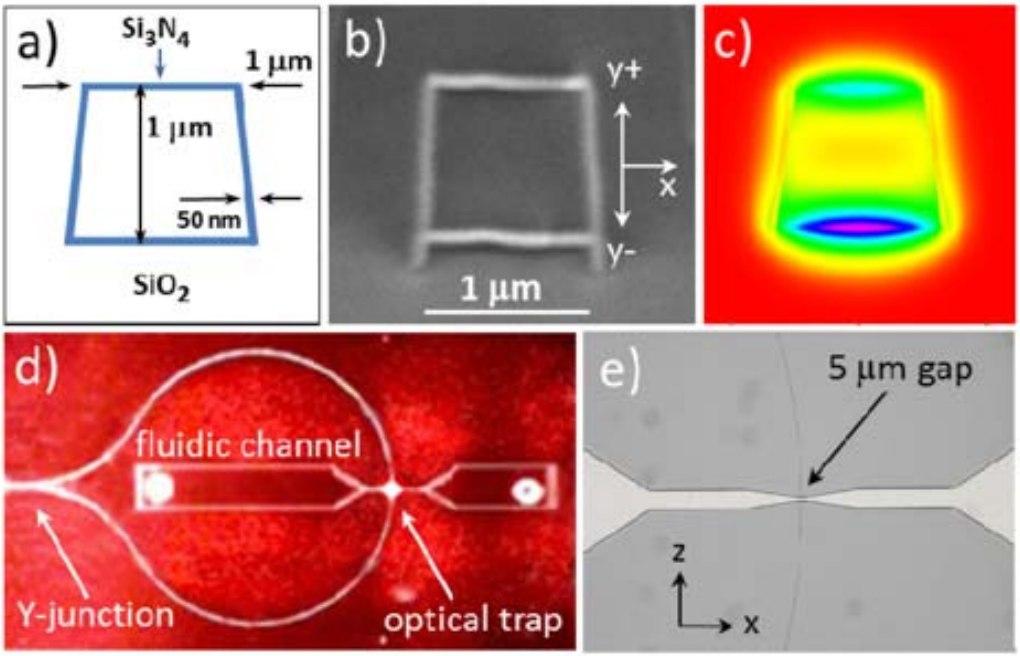

Fig. 19. *(a) Trapezoidal box shape Si_3N_4 waveguide design. (b) Cross-sectional SEM picture and (c) mode profile of the lowest TE mode in the waveguide. (d) Microscope image of the Raman trapping. (e) Microscope image of the central region of the device. Reprinted with permission from [128], ©OSA 2014.*

fluorescent lines 405, 488, 562, and 638 nm. These wavelengths can be combined using an integrated laser beam combiner (ILBC) [129] into one single-mode fiber [130] and is built out of several stages of wavelength-dependent components, such as bus-coupled resonators, MZIs, and AWGs [131]. The laser beam combiner in Fig. 20 shows

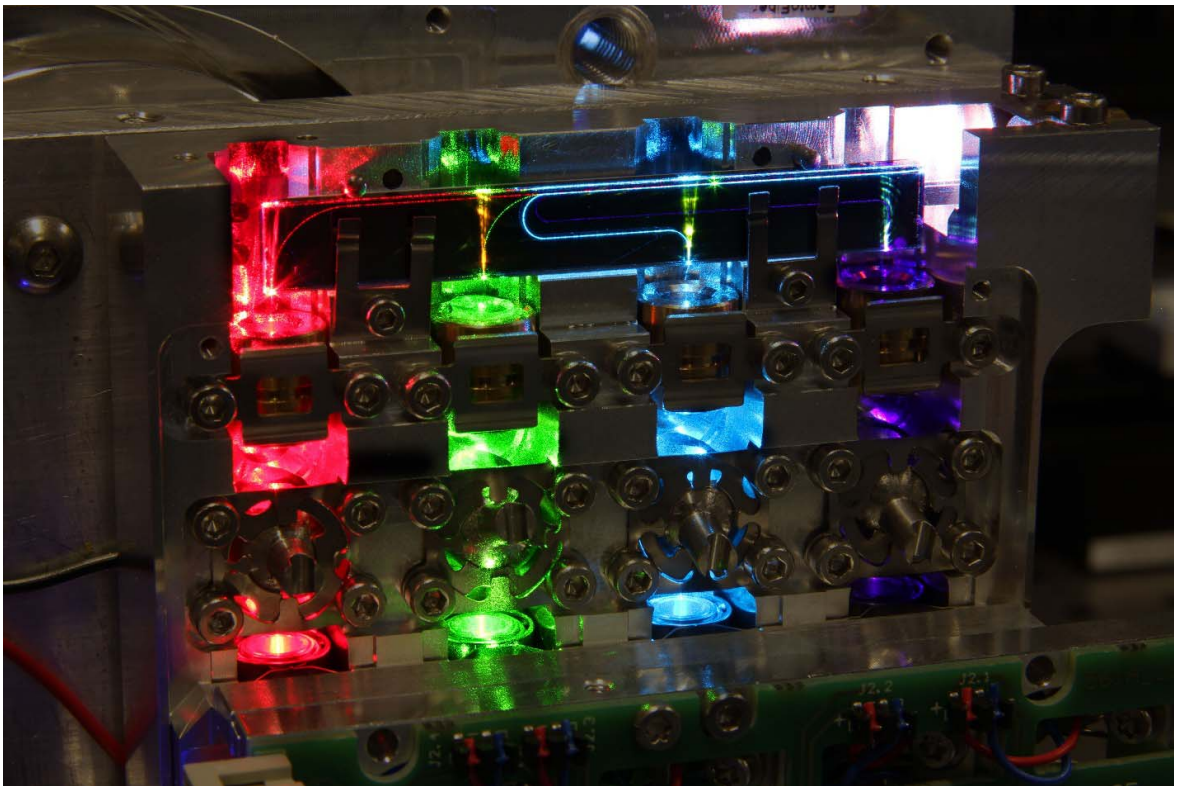

Fig. 20. *Photograph of integrated laser beam combiner for multiwavelength source from [132]. Image reprinted from [84], ©Wiley-VCH Verlag GmbH & Co. KGaA. Reproduced with permission.*

a photograph of the Si_3N_4combiner, four visible wavelength laser diodes, and the coupling optics within a 10×10 cm area [132]. Other imaging applications that have employed Si_3N_4 include optical coherence tomography (OCT) for noninvasive 3-D imaging of biological structures [133].

H. Other Applications

A wealth of other applications are poised to benefit from the attributes and performance of Si_3N_4 photonics, with state-of-the-art demonstrations including integrated optical gyros [134], [135], quantum communications [8], [136], NIR spectrometers for large ground- and space-based astronomical telescopes [137], and LIDAR [138].

VI. DISCUSSION AND FUTURE PROSPECTS

In this paper, we have reviewed the history and background of the silicon nitride (Si_3N_4) planar waveguide platform. When combined with SOI and III–V devices, the three platforms together open up a whole new generation of applications and system-on-chip applications. Low optical losses, transparency from visible through the MIR, compatibility with CMOS and wafer-scale foundry processes, and high power handling capabilities are among the key attributes of this system.

The broad design parameter space, possible within a single platform, gives designers access to linear and nonlinear PICs. A broad set of building blocks including ultrahigh Q resonators, ultranarrow tunable filters, narrow linewidth and tunable lasers, tunable analog RF and optical signal processing circuits, and true time delays are available in this technology. A wide array of applications will benefit from the optical transparency and low loss from the visible out to the IR, including optical inertial rotation sensors, microwave synthesizers, quantum communications, biophotonics, and nanoparticle analysis applications.

The successful transfer of this platform to the foundry as well as availability of PDK toolkits has moved this technology from the research labs to the development and commercialization stages. Future prospects include more sophisticated integration of linear and nonlinear functions as well as low-energy, high-speed tuning and modulation, and application to emerging applications such as neuromorphic computing and quantum computation.

REFERENCES

[1] C. Doerr, "Silicon photonic integration in telecommunications," *Frontiers Phys.*, vol. 3, p. 37, Aug. 2015.

[2] J. F. Bauters *et al.*, "Ultra-low loss silica-based waveguides with millimeter bend radius," in *Proc. 36th Eur. Conf. Opt. Commun.*, Sep. 2010, pp. 1–3.

[3] K. De Vos, I. Bartolozzi, E. Schacht, P. Bienstman, and R. Baets, "Silicon-on-insulator microring resonator for sensitive and label-free biosensing," *Opt. Express*, vol. 15, no. 12, pp. 7610–7615, Jun. 2007.

[4] G. A. Sanders, "Fiber optic gyro development at Honeywell," *Proc. SPIE*, vol. 9852, pp. 985207-1–985207-14, May 2016.

[5] J. Li, H. Lee, and K. J. Vahala, "Microwave synthesizer using an on-chip Brillouin oscillator," *Nature Commun.*, vol. 4, no. 12, p. 2097, Jun. 2013.

[6] M. Boerkamp *et al.*, "On-chip optical trapping and Raman spectroscopy using a TripleX dual-waveguide trap," *Opt. Express*, vol. 22, no. 25, pp. 30528–30537, 2014.

[7] D. Marpaung, C. Roeloffzen, R. Heideman, A. Leinse, S. Sales, and J. Capmany, "Integrated microwave photonics," *Lasers Photon. Rev.*, vol. 7, no. 4, pp. 506–538, Jul. 2013.

[8] A. Politi, M. J. Cryan, J. G. Rarity, S. Yu, and J. L. O'Brien, "Silica-on-silicon waveguide quantum circuits," *Science*, vol. 320, no. 5876, pp. 646–649, 2008.

[9] A. D. Ludlow, M. M. Boyd, J. Ye, E. Peik, and P. O. Schmidt, "Optical atomic clocks," *Rev. Mod. Phys.*, vol. 87, no. 2, pp. 637–701, 2015.

[10] M. Smit *et al.*, "An introduction to InP-based generic integration technology," *Semicond. Sci. Technol.*, vol. 29, no. 8, p. 083001, 2014.

[11] D. D'Agostino *et al.*, "Low-loss passive waveguides in a generic InP foundry process via local diffusion of zinc," *Opt. Express*, vol. 23, no. 19, pp. 25143–25157, 2015.

[12] D. L. Harame, L. J. Bousse, J. D. Shott, and J. D. Meindl, "Ion-sensing devices with silicon nitride and borosilicate glass insulators," *IEEE Trans. Electron Devices*, vol. 34, no. 8, pp. 1700–1707, Aug. 1987.

[13] K. Wörhoff, R. G. Heideman, A. Leinse, and M. Hoekman, "TriPleX: A versatile dielectric photonic platform," *Adv. Opt. Technol.*, vol. 4, no. 2, pp. 189–207, 2015.

[14] T. A. Huffman, G. M. Brodnik, C. Pinho, S. Gundavarapu, D. Baney, and D. J. Blumenthal, "Integrated resonators in an ultralow loss Si3N4/SiO2 platform for multifunction applications," *IEEE J. Sel. Topics Quantum Electron.*, vol. 24, no. 4, Jul./Aug. 2018, Art. no. 5900209.

[15] M. A. Tran, D. Huang, T. Komljenovic, J. Peters, A. Malik, and J. Bowers, "Ultra-low-loss silicon waveguides for heterogeneously integrated silicon/III-V photonics," *Appl. Sci.*, 2018.

[16] P. Muñoz *et al.*, "State of the art of silicon nitride photonics integration platforms," in *Proc. 19th Int. Conf. Transp. Opt. Netw. (ICTON)*, Jul. 2017, pp. 1–4.

[17] D. J. Blumenthal, C. Ciminelli, M. Dagenais, B. Eggleton, and D. V. Thourhout, "Introduction to the special issue on ultralow loss planar waveguides and their applications," *IEEE J. Sel. Topics Quantum Electron.*, vol. 24, no. 4, Jul./Aug. 2018, Art. no. 0200603.

[18] J. T. Boyd and C. S. Kuo, "Composite prism–grating coupler for coupling light into high refractive index thin-film waveguides," *Appl. Opt.*, vol. 15, no. 7, pp. 1681-1–1683, 1976.

[19] W. Stutius and W. Streifer, "Silicon nitride films on silicon for optical waveguides," *Appl. Opt.*, vol. 16, no. 12, pp. 3218–3222, 1977.

[20] J. T. Boyd, "Planar and channel optical waveguides utilizing silicon technology," *Proc. SPIE*, vol. 517, pp. 100–106, Jan. 1985.

[21] J. Cardenas, C. B. Poitras, J. T. Robinson, K. Preston, L. Chen, and M. Lipson, "Low loss etchless silicon photonic waveguides," *Opt. Express*, vol. 17, no. 6, pp. 4752–4757, Mar. 2009.

[22] S. Makovejs *et al.*, "Record-low (0.1460 dB/km) attenuation ultra-large aeff optical fiber for submarine applications," in *Proc. Opt. Fiber Commun. Conf. Post Deadline Papers*, Los Angeles, CA, USA: OSA, Mar. 2015, pp. 1–3.

[23] C. H. Henry, R. F. Kazarinov, H. J. Lee, K. J. Orlowsky, and L. E. Katz, "Low loss Si3N4-SiO2 optical waveguides on Si," *Appl. Opt.*, vol. 26, no. 13, pp. 2621–2624, 1987.

[24] R. G. Heideman, R. P. H. Kooyman, and J. Greve, "Performance of a highly sensitive optical waveguide Mach–Zehnder interferometer immunosensor," *Sens. Actuators B, Chem.*, vol. 10, no. 3, pp. 209–217, Feb. 1993.

[25] K. Wörhoff, P. V. Lambeck, H. Albers, O. Noordman, N. F. van Hulst, and T. J. A. Popma, "Optimization of LPCVD silicon oxynitride growth to large refractive index homogeneity and layer thickness uniformity," *Proc. SPIE*, vol. 3099, pp. 257–269, Sep. 1997.

[26] K. Wörhoff, A. Driessen, P. V. Lambeck, L. T. H. Hilderink, P. W. C. Linders, and T. J. A. Popma, "Plasma enhanced chemical vapor deposition silicon oxynitride optimized for application in integrated optics," *Sens. Actuators A, Phys.*, vol. 74, nos. 1–3, pp. 9–12, Apr. 1999.

[27] D. J. Blumenthal, "Routing packets with light," *Sci. Amer.*, vol. 284, no. 1, pp. 96–99, 2001.

[28] J. S. Barton *et al.*, "Recent progress on LASOR optical router and related integrated technologies," in *Proc. Int. Conf. Photon. Switching*, Aug. 2008, pp. 1–2.

[29] D. J. Blumenthal *et al.*, "Integrated photonics for low-power packet networking," *IEEE J. Sel. Topics Quantum Electron.*, vol. 17, no. 2, pp. 458–471, Mar. 2011.

[30] E. F. Burmeister *et al.*, "Photonic integrated circuit optical buffer for packet-switched networks," *Opt. Express*, vol. 17, no. 8, pp. 6629–6635, 2009.

[31] C. H. Cox and E. I. Ackerman, "Microwave photonics: Past, present and future," in *Proc. Int. Top. Meeting Microw. Photon. Jointly Held Asia–Pacific Microw. Photon. Conf.*, Sep./Oct. 2008, pp. 9–11.

[32] A. J. Seeds and K. J. Williams, "Microwave photonics," *J. Lightw. Technol.*, vol. 24, no. 12, pp. 4628–4641, Dec. 2006.

[33] W. Ng, A. A. Walston, G. L. Tangonan, J. J. Lee, I. L. Newberg, and N. Bernstein, "The first demonstration of an optically steered microwave phased array antenna using true-time-delay," *J. Lightw. Technol.*, vol. 9, no. 9, pp. 1124–1131, Sep. 1991.

[34] J. Buus M. Amann, and D. Blumenthal, "Communications applicationsand requirements," Tech. Rep., 2009.

[35] J. Bauters *et al.*, "Planar waveguides with less than 0.1 dB/m propagation loss fabricated with wafer bonding," *Opt. Express*, vol. 19, no. 24, pp. 24090–24101, 2011.

[36] J. F. Bauters *et al.*, "A comparison of approaches for ultra-low-loss waveguides," in *Proc. Opt. Fiber Commun. Conf.* Los Angeles, CA, USA: OSA, Mar. 2012, pp. 1–3.

[37] M.-C. Tien, J. F. Bauters, M. J. R. Heck, D. J. Blumenthal, and J. E. Bowers, "Ultra-low loss Si3N4 waveguides with low nonlinearity and high power handling capability," *Opt. Express*, vol. 18, no. 23, pp. 23562–23568, 2010.

[38] J. F. Bauters, M. J. R. Heck, D. Dai, J. S. Barton, D. J. Blumenthal, and J. E. Bowers, "Ultralow-loss planar Si3N4 waveguide polarizers," *IEEE Photon. J.*, vol. 5, no. 1, Feb. 2013, Art. no. 6600207.

[39] R. G. Heideman and P. V. Lambeck, "Remote opto-chemical sensing with extreme sensitivity: Design, fabrication and performance of a pigtailed integrated optical phase-modulated Mach–Zehnder interferometer system," *Sens. Actuators B, Chem.*, vol. 61, nos. 1–3, pp. 100–127, Dec. 1999.

[40] F. Morichetti *et al.*, "Box-shaped dielectric waveguides: A new concept in integrated optics?" *J. Lightw. Technol.*, vol. 25, no. 9, pp. 2579–2589, Sep. 2007.

[41] J. P. Epping *et al.*, "On-chip visible-to-infrared supercontinuum generation with more than 495 THz spectral bandwidth," *Opt. Express*, vol. 23, no. 15, pp. 19596–19604, 2015.

[42] M. H. P. Pfeiffer *et al.*, "Photonic Damascene process for integrated high-Q microresonator based nonlinear photonics," *Optica*, vol. 3, no. 1, pp. 20–25, 2016.

[43] K. Luke, A. Dutt, C. B. Poitras, and M. Lipson, "Overcoming Si_3N_4 film stress limitations for high quality factor ring resonators," *Opt. Express*, vol. 21, no. 19, pp. 22829–22833, Sep. 2013.

[44] Service, L.I.M.P.W. [Online]. Available: https://photonics.lionix-international.com/mpw-service/

[45] MPW, L. [Online]. Available: https://www.ligentec.com/services/foundry/mpw/

[46] PIX4life. *PIX4life*. [Online]. Available: http://pix4life.eu

[47] IMB-CNM, I.o.M.o.B. *Silicon Nitride Photonic Integration Platform*. [Online]. Available: http://www.imb-cnm.csic.es/index.php/en/clean-room/silicon-nitride-technology

[48] A. Driessen, H. M. M. K. Koerkamp, and T. J. A. Popma, "Novel integrated optic intensity modulator based on mode coupling," *Fiber Integr. Opt.*, vol. 13, no. 4, pp. 445–461, 1994.

[49] R. M. de Ridder, K. Warhoff, A. Driessen, P. V. Lambeck, and H. Albers, "Silicon oxynitride planar waveguiding structures for application in optical communication," *IEEE J. Sel. Topics Quantum Electron.*, vol. 4, no. 6, pp. 930–937, Nov./Dec. 1998.

[50] R. G. Heideman, R. P. H. Kooyman, and J. Greve, "Immunoreactivity of adsorbed anti human chorionic gonadotropin studied with an optical waveguide interferometric sensor," *Biosensors Bioelectron.*, vol. 9, no. 1, pp. 33–43, 1994.

[51] P. Del'Haye, A. Schliesser, O. Arcizet, T. Wilken, R. Holzwarth, and T. J. Kippenberg, "Optical frequency comb generation from a monolithic microresonator," *Nature*, vol. 450, pp. 1214–1217, Dec. 2007.

[52] C. G. H. Roeloffzen, "Low-loss Si3N4 TriPleX optical waveguides: Technology and applications overview," *IEEE J. Sel. Topics Quantum Electron.*, vol. 24, no. 4, Jul./Aug. 2018, Art. no. 4400321.

[53] J. F. Bauters *et al.*, "Ultra-low-loss high-aspect-ratio Si3N4 waveguides," *Opt. Express*, vol. 19, no. 4, pp. 3163–3174, 2011.

[54] M. H. P. Pfeiffer *et al.*, "Photonic damascene process for low-loss, high-confinement silicon nitride waveguides," *IEEE J. Sel. Topics Quantum Electron.*, vol. 24, no. 4, Aug. 2018, Art. no. 6101411.

[55] J. F. Bauters *et al.*, "Ultra-low-loss high-aspect-ratio Si3N4 waveguides," *Opt. Express*, vol. 19, no. 4, pp. 3163–3174, 2011.

[56] R. L. Moreira, "Integrated optical delay line circuits on a ultra-low loss planar waveguide platform," Dept. Elect. Comput. Eng., Univ. California, Santa Barbara, Santa Barbara, CA, USA, Tech. Rep., 2016.

[57] D. T. Spencer, J. F. Bauters, M. J. R. Heck, and J. E. Bowers, "Integrated waveguide coupled Si3N4 resonators in the ultrahigh-Q regime," *Optica*, vol. 1, no. 3, pp. 153–157, 2014.

[58] L. Zhuang, D. Marpaung, M. Burla, W. Beeker, A. Leinse, and C. Roeloffzen, "Low-loss, high-index-contrast Si3N4/SiO2 optical waveguides for optical delay lines in microwave photonics signal processing," *Opt. Express*, vol. 19, no. 23, pp. 23162–23170, 2011.

[59] D. J. Blumenthal, "Ultra-low loss SiN waveguide platform for integrated passive and active components for next generation photonic integrated circuits," in *Proc. Summer Top. Meeting*, HI, USA, 2016, Paper WA2.4.

[60] C. Roeloffzen *et al.*, "Enhanced coverage though optical beamforming in fiber wireless networks," in *Proc. 19th Int. Conf. Transparent Opt. Netw. (ICTON)*, Jul. 2017, pp. 1–4.

[61] N. Hosseini *et al.*, "Stress-optic modulator in TriPleX platform using a piezoelectric lead zirconate titanate (PZT) thin film," *Opt. Express*, vol. 23, no. 11, pp. 14018–14026, 2015.

[62] J. P. Epping *et al.*, "Ultra-low-power stress-optics modulator for microwave photonics," *Proc. SPIE*, vol. 10106, pp. 101060F-1–101060F-8, Feb. 2017.

[63] D. H. A. Blank, M. Dekkers, and G. Rijnders, "Pulsed laser deposition in Twente: From research tool towards industrial deposition," *J. Phys. D, Appl. Phys.*, vol. 47, no. 3, p. 034006, 2014.

[64] J. S. Levy, A. Gondarenko, M. A. Foster, A. C. Turner-Foster, A. L. Gaeta, and M. Lipson, "CMOS-compatible multiple-wavelength oscillator for on-chip optical interconnects," *Nature Photon.*, vol. 4, pp. 37–40, Dec. 2009.

[65] S. Darmawan and M. K. Chin, "Critical coupling, oscillation, reflection, and transmission in optical waveguide-ring resonator systems," *J. Opt. Soc. Amer. B, Opt. Phys.*, vol. 23, no. 5, pp. 834–841, 2006.

[66] S. Gundavarapu *et al.* (2017). "Integrated waveguide Brillouin laser." [Online]. Available: https://arxiv.org/abs/1709.04512

[67] P. Xing, G. F. R. Chen, X. Zhao, D. K. T. Ng, M. C. Tan, and D. T. H. Tan, "Silicon rich nitride ring resonators for rare—Earth doped telecommunications-band amplifiers pumped at the O-band," *Sci. Rep.*, vol. 7, Aug. 2017, Art. no. 9101.

[68] M. Belt *et al.*, "Sidewall gratings in ultra-low-loss Si3N4 planar waveguides," *Opt. Express*, vol. 21, no. 1, pp. 1181–1188, 2013.

[69] J. D. B. Bradley, L. Agazzi, D. Geskus, F. Ay, K. Wörhoff, and M. Pollnau, "Gain bandwidth of 80 nm and 2 dB/cm peak gain in Al2O3:Er^{3+} optical amplifiers on silicon," *J. Opt. Soc. Amer. B, Opt. Phys.*, vol. 27, no. 2, pp. 187–196, 2010.

[70] E. H. Bernhardi *et al.*, "Ultra-narrow-linewidth, single-frequency distributed feedback waveguide laser in Al2O3:Er^{3+} on silicon," *Opt. Lett.*, vol. 35, no. 14, pp. 2394–2396, 2010.

[71] M. Belt, T. Huffman, M. L. Davenport, W. Li, J. S. Barton, and D. J. Blumenthal, "Arrayed narrow linewidth erbium-doped waveguide-distributed feedback lasers on an ultra-low-loss silicon-nitride platform," *Opt. Lett.*, vol. 38, no. 22, pp. 4825–4828, 2013.

[72] M. Belt and D. J. Blumenthal, "Erbium-doped waveguide DBR and DFB laser arrays integrated within an ultra-low-loss Si3N4 platform," *Opt. Express*, vol. 22, no. 9, pp. 10655–10660, 2014.

[73] Purnawirman, "Erbium-doped laser with multi-segmented silicon nitride structure," in *Proc. Opt. Fiber Commun. Conf.*, San Francisco, CA, USA, Mar. 2014, pp. 1–3.

[74] E. S. Hosseini *et al.*, "CMOS-compatible 75 mW erbium-doped distributed feedback laser," *Opt. Lett.*, vol. 39, no. 11, pp. 3106–3109, 2014.

[75] M. Belt, "Optically pumped ultra-low loss waveguide lasers and amplifiers," Dept. Elect. Comput. Eng., Univ. California, Santa Barbara, Santa Barbara, CA, USA, Tech. Rep., 2017.

[76] Y. Zhu, "Hybrid colloidal quantum dot silicon nitride waveguide gain measurement based on variable stripe length method," in *Proc. Conf. Lasers Electro-Opt.*, San Jose, CA, USA, Jun. 2016, pp. 1–2.

[77] W. Xie *et al.*, "Integrated silicon nitride microdisk lasers based on quantum dots," in *Proc. Conf. Lasers Electro-Opt.*, San Jose, CA, USA, Jun. 2016, pp. 1–2.

[78] A. Z. Subramanian *et al.*, "Silicon and silicon nitride photonic circuits for spectroscopic sensing on-a-chip [Invited]," *Photon. Res.*, vol. 3, no. 5, pp. B47–B59, 2015.

[79] Y. Liu, A. Choudhary, D. Marpaung, and B. J. Eggleton, "Gigahertz optical tuning of an on-chip radio frequency photonic delay line," *Optica*, vol. 4, no. 4, pp. 418–423, 2017.

[80] R. Heideman, M. Hoekman, and E. Schreuder, "TriPleX-based integrated optical ring resonators for lab-on-a-chip and environmental detection," *IEEE J. Sel. Topics Quantum Electron.*, vol. 18, no. 5, pp. 1583–1596, Sep./Oct. 2012.

[81] P. A. Morton, M. J. Morton, and S. J. Morton, "Ultra low phase noise, high power, hybrid lasers for RF mixing and optical sensing applications," in *Proc. IEEE Avionics Vehicle Fiber-Opt. Photon. Conf. (AVFOP)*, Nov. 2017, pp. 1–2.

[82] B. Stern, X. Ji, A. Dutt, and M. Lipson, "Compact narrow-linewidth integrated laser based on a low-loss silicon nitride ring resonator," *Opt. Lett.*, vol. 42, no. 21, pp. 4541–4544, 2017.

[83] Y. Fan *et al.*, "290 Hz intrinsic linewidth from an integrated optical chip-based widely tunable InP-Si3N4hybrid laser," in *Proc. Conf. Lasers Electro-Opt.*, San Jose, CA, USA, Jun. 2017, p. 1.

[84] D. Geuzebroek, R. Dekker, and P. van Dijk, "Photonics packaging made visible," *Opt. Photon*, vol. 12, no. 5, pp. 34–38, Dec. 2017.

[85] Y. Kaneda *et al.*, "200-mW, narrow-linewidth 1064.2-nm Yb-doped fiber laser," in *Proc. Conf. Lasers Electro-Opt. (CLEO)*, May 2004, p. 2.

[86] M. Belt and D. J. Blumenthal, "High temperature operation of an integrated erbium-doped DBR laser on an ultra-low-loss Si3N4platform," in *Proc. Opt. Fiber Commun. Conf.*, Mar. 2015, pp. 1–3.

[87] J. Yao, "Microwave photonics," *J. Lightw. Technol.*, vol. 27, no. 3, pp. 314–335, Feb. 1, 2009.

[88] J. Capmany and D. Novak, "Microwave photonics combines two worlds," *Nature Photon.*, vol. 1, pp. 319–330, Jun. 2007.

[89] R. Gaudino, S. Han, M. Shell, M. D. Vaughn, D. J. Blumenthal, and J. Laskar, "A digital-baseband/SCM-control fiber unk with novel differential integrated optic transmitter and microwave/optical direct detection receiver," in *Proc. Int. Top. Meeting Microw. Photon. (MWP)*, Sep. 1997, pp. 193–196.

[90] A. Yariv, Y. Xu, R. K. Lee, and A. Scherer, "Coupled-resonator optical waveguide: A proposal and analysis," *Opt. Lett.*, vol. 24, no. 11, pp. 711–713, 1999.

[91] A. Melloni, R. Costa, P. Monguzzi, and M. Martinelli, "Ring-resonator filters in silicon oxynitride technology for dense wavelength-division multiplexing systems," *Opt. Lett.*, vol. 28, no. 17, pp. 1567–1569, 2003.

[92] A. Leinse *et al.*, "TriPleX waveguide platform: Low-loss technology over a wide wavelength range," *Proc. SPIE*, vol. 8767, pp. 87670E-1–87670E-13, 2013.

[93] C. Taddei *et al.*, "Fully reconfigurable coupled ring resonator-based bandpass filter for microwave signal processing," in *Proc. 9th Asia–Pacific Microw. Photon. Conf. (APMP) Int. Topical Meeting Microw. Photon. (MWP)*, Oct. 2014, pp. 44–47.

[94] L. Zhuang, C. G. H. Roeloffzen, M. Hoekman, K.-J. Boller, and A. J. Lowery, "Programmable photonic signal processor chip for radiofrequency applications," *Optica*, vol. 2, no. 10, pp. 854–859, 2015.

[95] J. Capmany, B. Ortega, D. Pastor, and S. Sales, "Discrete-time optical processing of microwave signals," *J. Lightw. Technol.*, vol. 23, no. 2, pp. 702–723, Feb. 2005.

[96] C. G. H. Roeloffzen, L. Zhuang, R. G. Heideman, A. Borreman, and W. van Etten, "Ring

resonator-based tunable optical delay line in LPCVD waveguide technology," in *Proc. Symp. IEEE/LEOS Benelux Chapter*. Mons, Belgium: Faculte Polytechnique de Mons, 2005, pp. 1–4.
[97] T. Huffman, M. Davenport, M. Belt, J. E. Bowers, D. J. Blumenthal, "Ultra-low loss large area waveguide coils for integrated optical gyroscopes," *IEEE Photon. Technol. Lett.*, vol. 29, no. 2, pp. 185–188, Jan. 15, 2017.
[98] C. G. H. Roeloffzen *et al.*, "Silicon nitride microwave photonic circuits," *Opt. Exp.*, vol. 21, no. 19, pp. 22937–22961, Jun. 2013.
[99] R. L. Moreira *et al.*, "Integrated ultra-low-loss 4-bit tunable delay for broadband phased array antenna applications," *IEEE Photon. Technol. Lett.*, vol. 25, no. 12, pp. 1165–1168, Jun. 15, 2013.
[100] R. Moreira, S. Gundavarapu, and D. Blumenthal, "Compact programmable monolithically integrated 10-stage multi-channel WDM dispersion equalizer on low-loss silicon nitride planar waveguide platform," in *Proc. Opt. Fiber Commun. Conf. Exhib. (OFC)*, Mar. 2015, pp. 1–3.
[101] R. Moreira, S. Gundavarapu, and D. J. Blumenthal, "Programmable eye-opener lattice filter for multi-channel dispersion compensation using an integrated compact low-loss silicon nitride platform," *Opt. Express*, vol. 24, no. 15, pp. 16732–16742, 2016.
[102] G. M. Brodnik, C. Pinho, F. Chang, and D. J. Blumenthal, "Extended reach 40km transmission of C-band real-time 53.125 Gbps PAM-4 enabled with a photonic integrated tunable lattice filter dispersion compensator," in *Proc. Opt. Fiber Commun. Conf.* San Diego, CA, USA: OSA, Mar. 2018, pp. 1–3.
[103] D. J. Jones *et al.*, "Carrier-envelope phase control of femtosecond mode-locked lasers and direct optical frequency synthesis," *Science*, vol. 288, no. 5466, pp. 635–639, 2000.
[104] Z. Wang *et al.*, "A III-V-on-Si ultra-dense comb laser," *Light, Sci. Appl.*, vol. 6, p. e16260, May 2017.
[105] C. Weimann *et al.*, "Silicon-organic hybrid (SOH) frequency comb sources for terabit/s data transmission," *Opt. Express*, vol. 22, no. 3, pp. 3629–3637, 2014.
[106] J. Pfeifle, "Flexible terabit/s Nyquist-WDM super-channels using a gain-switched comb source," *Opt. Express*, vol. 23, no. 2, pp. 724–738, 2015.
[107] T. J. Kippenberg, R. Holzwarth, and S. A. Diddams, "Microresonator-based optical frequency combs," *Science*, vol. 332, no. 6029, pp. 555–559, 2011.
[108] M. A. Foster, J. S. Levy, O. Kuzucu, K. Saha, M. Lipson, and A. L. Gaeta, "Silicon-based monolithic optical frequency comb source," *Opt. Express*, vol. 19, no. 15, pp. 14233–14239, 2011.
[109] T. Herr *et al.*, "Temporal solitons in optical microresonators," *Nature Photon.*, vol. 8, pp. 145–152, Dec. 2013.
[110] P. Marin-Palomo *et al.*, "Microresonator-based solitons for massively parallel coherent optical communications," *Nature*, vol. 546, pp. 274–279, Jun. 2017.
[111] J. Pfeifle *et al.*, "Coherent terabit communications with microresonator Kerr frequency combs," *Nature Photon.*, vol. 8, pp. 375–380, Apr. 2014.
[112] C. Koos *et al.*, "Chip-scale frequency comb generators for high-speed communications and optical metrology," *Proc. SPIE*, vol. 10090, p. 10090, Feb. 2017.
[113] R. Halir, Y. Okawachi, J. S. Levy, M. A. Foster, M. Lipson, and A. L. Gaeta, "Ultrabroadband supercontinuum generation in a CMOS-compatible platform," *Opt. Lett.*, vol. 37, no. 10, pp. 1685–1687, 2012.
[114] J. M. C. Boggio *et al.*, "Dispersion engineered silicon nitride waveguides by geometrical and refractive-index optimization," *J. Opt. Soc. Amer. B, Opt. Phys.*, vol. 31, no. 11, pp. 2846–2857, 2014.
[115] H. Zhao *et al.*, "Visible-to-near-infrared octave spanning supercontinuum generation in a silicon nitride waveguide," *Opt. Lett.*, vol. 40, no. 10, pp. 2177–2180, 2015.
[116] A. Klenner *et al.*, "Gigahertz frequency comb offset stabilization based on supercontinuum generation in silicon nitride waveguides," *Opt. Express*, vol. 24, no. 10, pp. 11043–11053, 2016.
[117] D. R. Carlson, "Self-referenced frequency combs using high-efficiency silicon-nitride waveguides," *Opt. Lett.*, vol. 42, no. 12, pp. 2314–2317, 2017.
[118] M. A. G. Porcel, "Two-octave spanning supercontinuum generation in stoichiometric silicon nitride waveguides pumped at telecom wavelengths," *Opt. Express*, vol. 25, no. 2, pp. 1542–1554, 2017.
[119] D. Geuzebroek, A. van Rees, E. Klein, and K. Lawniczuk, "Ultra-wide band (400-1700 nm) integrated spectrometer based on arrayed waveguide gratings for spectral tissue sensing," in *Proc. IEEE 14th Int. Conf. Group IV Photon. (GFP)*, Aug. 2017, pp. 83–84.
[120] D. Geuzebroek, A. van Rees, E. Klein, and K. Lawniczuk, "Visible arrayed waveguide grating (400nm–700nm) for ultra-wide band (400–1700nm) integrated spectrometer for spectral tissue sensing," in *Proc. Eur. Conf. Lasers Electro-Optics Eur. Quantum Electron. Conf.* Munich, Germany: OSA, Jun. 2017, p. 1.
[121] A. Q. Liu, H. J. Huang, L. K. Chin, Y. F. Yu, and X. C. Li, "Label-free detection with micro optical fluidic systems (MOFS): A review," *Anal. Bioanal. Chem.*, vol. 391, no. 7, pp. 2443–2452, 2008.
[122] J. Yue, F. H. Falke, J. C. Schouten, and T. A. Nijhuis, "Microreactors with integrated UV/Vis spectroscopic detection for online process analysis under segmented flow," *Lab Chip*, vol. 13, no. 24, pp. 4855–4863, 2013.
[123] A. Dhakal, F. Peyskens, A. Z. Subramanian, N. Le Thomas, and R. Baets, "Enhanced spontaneous raman signal collected evanescently by silicon nitride slot waveguides," in *Proc. CLEO*. San Jose, CA, USA: OSA, 2015, Paper STh4H.3.
[124] C. A. Barrios *et al.*, "Slot-waveguide biochemical sensor," *Opt. Lett.*, vol. 32, pp. 3080–3082, Oct. 2007.
[125] G. A. J. Besselink, R. G. Heideman, E. Schreuder, L. S. Wevers, F. Falke, and H. Van den Vleckkert, "Performance of arrayed microring resonator sensors with the TriPleX platform," *J. Biosens. Bioelectron.*, vol. 7, no. 2, pp. 1–11, Jul. 2016.
[126] K. Kneipp, H. Kneipp, I. Itzkan, R. R. Dasari, and M. S. Feld, "Ultrasensitive chemical analysis by raman spectroscopy," *Chem. Rev.*, vol. 99, no. 10, pp. 2957–2976, 1999.
[127] S. Pathak, P. Dumon, D. V. Thourhout, and W. Bogaerts, "Comparison of AWGs and echelle gratings for wavelength division multiplexing on silicon-on-insulator," *IEEE Photon. J.*, vol. 6, no. 5, pp. 1–9, Oct. 2014.
[128] M. Boerkamp *et al.*, "On-chip optical trapping and Raman spectroscopy using a TripleX dual-waveguide trap," *Opt. Express*, vol. 22, no. 25, pp. 30528–30537, Dec. 2014.
[129] A. Leinse *et al.*, "TriPleX waveguide platform: Low-loss technology over a wide wavelength range," *Proc. SPIE*, vol. 8767, p. 87670E, May 2013.
[130] R. Dekker, E. J. Klein, and D. H. Geuzebroek, "Polarization maintaining single mode color combining using TriPleX based integrated optics for biophotonic applications," in *Proc. IEEE Photon. Conf.*, Sep. 2012, pp. 286–287.
[131] D. Geuzebroek, R. Dekker, E. Klein, and J. van Kerkhof, "Photonic integrated circuits for visible light and near infrared: Controlling transport and properties of light," *Sens. Actuators B, Chem.*, vol. 223, pp. 952–956, Feb. 2016.
[132] S. Romero-García *et al.*, "Photonic integrated circuits for multi-color laser engines," *Proc. SPIE*, vol. 10108, p. 101080Z, Mar. 2017.
[133] A. Leinse *et al.*, "Spectral domain, common path OCT in a handheld PIC based system," *Proc. SPIE*, vol. 10483, p. 104831J, Feb. 2018.
[134] S. Srinivasan *et al.*, "Design of integrated hybrid silicon waveguide optical gyroscope," *Opt. Express*, vol. 22, no. 21, pp. 24988–24993, 2014.
[135] S. Gundavarapu *et al.*, "Integrated ultra-low-loss silicon nitride waveguide coil for optical gyroscopes," in *Proc. Opt. Fiber Commun. Conf. Exhib. (OFC)*, Mar. 2016, pp. 1–3.
[136] O. Adeline and D. Eleni, "Recent advances on integrated quantum communications," *J. Opt.*, vol. 18, no. 8, p. 083002, 2016.
[137] P. Gatkine, S. Veilleux, Y. Hu, J. Bland-Hawthorn, and M. Dagenais, "Arrayed waveguide grating spectrometers for astronomical applications: New results," *Opt. Express*, vol. 25, no. 15, pp. 17918–17935, 2017.
[138] C. V. Poulton *et al.*, "Large-scale silicon nitride nanophotonic phased arrays at infrared and visible wavelengths," *Opt. Lett.*, vol. 42, no. 1, pp. 21–24, 2017.

ABOUT THE AUTHORS

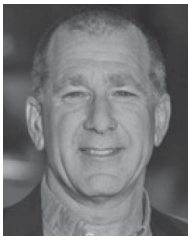

Daniel J. Blumenthal (Fellow, IEEE) received the B.S.E.E. degree from the University of Rochester, Rochester, NY, USA, the M.S.E.E. degree from Columbia University, New York, NY, USA, and the Ph.D. degree from the University of Colorado at Boulder, Boulder, CO, USA, in 1993.

He is currently a Professor in the Department of Electrical and Computer Engineering at the University of California Santa Barbara (UCSB), Santa Barbara, CA, USA and Director of the Terabit Optical Ethernet Center (TOEC) and heads the Optical Communications and Photonics Integration (OCPI) group (ocpi.ece.ucsb.edu). He is cofounder of Packet Photonics and Calient Networks, startups for Telecommunications and Data-Communications. He holds 22 U.S. patents; has published over 410 papers in the areas of optical communications, optical networks, and packet nitride ultralow-loss waveguide (ULLW) and InP photonics circuits, and nanophotonic device technologies; and is coauthor of *Tunable Laser Diodes and Related Optical Sources* (New York, NY, USA: IEEE–Wiley, 2005).

Dr. Blumenthal is a Fellow of the National Academy of Inventors (NAI) and the Optical Society of America. He has served on the Board of Directors for National LambdaRail (NLR) and as an elected member of the Internet2 Architecture Advisory Council. He is a recipient of a Presidential Early Career Award for Scientists and Engineers (PECASE), a National Science Foundation Young Investigator Award (NYI), and an Office of Naval Research Young Investigator Program (YIP) Award. He has served on numerous program committees including OFC, Photonics in Switching and as general editor of multiple IEEE journals including the 2018 IEEE Journal on Selected Areas in Quantum Electronics Special Issue on Ultra-Low Loss Planar Silicon Nitride Waveguides and Their Applications.

René Heideman received the M.Sc. and Ph.D. degrees in applied physics from the University of Twente, Enschede, The Netherlands, in August 1988 and January 1993, respectively.

He is an expert in the field of MST, with more than 25 years of experience. He specializes in integrated optics (IO), covering both (bio) chemical sensing and telecom applications. He is the inventor of the TriPleX technology, (co)author of more than 250 papers and holds more than 25 patents in the IO field, on more than ten different subjects. From 2001 to 2016, he was CTO of LioniX BV, which he cofounded in 2001. Since 2016, he has been CTO of LioniX International BV. Since 2008, he has been board member (CTO) of Panthera BV, a group of high-tech innovative companies focusing on creating new business based on micro/nanotechnology. Since June 2012, he has been a (visiting) Professor of Nanotechnology at Saxion University of Applied Sciences, Enschede, The Netherlands. He is a member of several Dutch and European steering committees and, among others, board member of MinacNed (Dutch association for microsystems and nanotechnology) and BOS-member of the European consortium Photonics21.

Arne Leinse was born in The Netherlands in 1977. He received the Master of Physics degree and the Ph.D. degree in the integrated optical microsystems group from the University Twente, Enschede, The Netherlands, in 2001 and 2005, respectively. His Ph.D. dissertation was titled "Polymeric microring resonator based electro-optic modulator."

He joined LioniX BV where he has been involved in the invention and development of the TriPleX platform from the beginning. He (co)authored more than 100 articles. He has been active in integrated optics for more than 15 years. He was the Vice-President of LioniX BV and has been with LioniX-International, Enschede, The Netherlands, since its establishment in 2016 and is currently a Chief Commercial Officer.

Douwe Geuzebroek received the Ph.D. degree in electrical engineering from the University of Twente, Enschede, The Netherlands, at the Integrated Optical MicroSystem (IOMS) group on a topic of applying integrated optical microring resonators in telecommunication networks.

Currently, he is is VP Marketing & Sales at LioniX International. He has over 15 years of experience in integrated photonics and its applications, ranching from R&D to product development stages. He has a strong interest in matching the technical aspect of a technology to the needs of the market. In 2005, he joined LioniX BV as a Design Engineer and Project Leader focusing on microring resonators and other integrated optical telecommunication devices and was actively involved in the startup of XiO Photonics in 2008. As VP Marketing and Sales at XiO Photonics, he supported the development of the waveguide technology for visible light applications and the introduction of this technology in several products. He participated in several research projects both national and European. Currently, as VP Marketing & Sales at LioniX International, he is involved in the acquisition of new commercial and research projects for photonic integrated modules in life science, metrology, and telecommunication applications.

Chris Roeloffzen received the M.Sc. degree in applied physics and the Ph.D. degree in electrical engineering from the University of Twente, Enschede, The Netherlands, in 1998 and 2002, respectively.

In 2002, he became an Assistant Professor in the Telecommunication Engineering Group, University of Twente, where he was involved in research and education on integrated microwave photonic systems. In 2009, he founded SATRAX, a spinoff of the University of Twente, where he was CTO. In 2017, SATRAX, LioniX, and XiO Photonics merged into LioniX International. He is now Chief Scientific Officer of LioniX International. He has authored or coauthored 40 refereed journal publications and more than 100 conference papers and delivered 13 invited talks at various international conferences.

Dr. Roeloffzen was the technical program committee (TPC) Co-Chair of the IEEE Topical Meeting of Microwave Photonics (MWP 2017). He is an MC member of the EU COST 16220: European Network for High Performance Integrated Microwave Photonics.